



Geobiology of the Late Paleoproterozoic Duck Creek Formation, Western Australia

Citation

Wilson, Jonathan P., Woodward W. Fischer, David T. Johnston, Andrew H. Knoll, John P. Grotzinger, Malcolm R. Walter, Neal J. McNaughton, et al. 2010. Geobiology of the late Paleoproterozoic Duck Creek Formation, Western Australia. *Precambrian Research* 179(1-4): 135-149.

Published Version

doi:10.1016/j.precamres.2010.02.019

Permanent link

<http://nrs.harvard.edu/urn-3:HUL.InstRepos:4795338>

Terms of Use

This article was downloaded from Harvard University's DASH repository, and is made available under the terms and conditions applicable to Open Access Policy Articles, as set forth at <http://nrs.harvard.edu/urn-3:HUL.InstRepos:dash.current.terms-of-use#OAP>

Share Your Story

The Harvard community has made this article openly available.
Please share how this access benefits you. [Submit a story](#).

[Accessibility](#)

**Geobiology of the Late Paleoproterozoic Duck Creek Formation, Western
Australia**

Jonathan P. Wilson^{1,2*}, Woodward W. Fischer², David T. Johnston¹, Andrew H. Knoll³,
John P. Grotzinger², Malcolm R. Walter⁵, Neal J. McNaughton⁹, Mel Simon⁴, John
Abelson⁴, Daniel P. Schrag¹, Roger Summons⁶, Abigail Allwood⁷, Miriam Andres⁸,
Crystal Gammon², Jessica Garvin, Sky Rashby², Maia Schweizer², Wesley A. Watters⁶

ABSTRACT

The ca. 1.8 Ga Duck Creek Formation, Western Australia, preserves 1000 m of carbonates and minor iron formation that accumulated along a late Paleoproterozoic ocean margin. Two upward-deepening stratigraphic packages are preserved, each characterized by peritidal precipitates at the base and iron formation and carbonate turbidites in its upper part. Consistent with recent studies of Neoarchean basins, carbon isotope ratios of Duck Creek carbonates show no evidence for a strong isotopic depth gradient, but carbonate minerals in iron formations can be markedly depleted in ¹³C. In contrast, oxygen isotopes covary strongly with depth; δ¹⁸O values as positive as 2‰ VPDB in peritidal facies systematically decline to values of -6 to -16‰ in basinal rocks,

* Corresponding author: jpwilson@caltech.edu

¹ Department of Earth and Planetary Sciences, Harvard University

² Division of Geological and Planetary Sciences, California Institute of Technology, Pasadena, CA USA

³ Department of Organismic and Evolutionary Biology, Harvard University

⁴ The Agouron Institute

⁵ Australian Centre for Astrobiology, University of New South Wales, Australia

⁶ Massachusetts Institute of Technology

⁷ Jet Propulsion Laboratory

⁸ Chevron Corp.

⁹ Curtin University of Technology, Australia

1 reflecting, we posit, the timing of diagenetic closure. The Duck Creek Formation
2 contains microfossils similar to those of the Gunflint Formation, Canada; they are
3 restricted to early diagenetic cherts developed in basinal facies, strengthening the
4 hypothesis that such fossils capture communities driven by iron metabolism. Indeed, X-
5 ray diffraction data indicate that the Duck Creek basin was ferruginous throughout its
6 history. The persistence of ferruginous waters and iron formation deposition in Western
7 Australia for at least several tens of millions of years after the transition to sulfidic
8 conditions in Laurentia suggests that the late Paleoproterozoic expansion of sulfidic
9 subsurface waters was globally asynchronous.

11
12 Keywords: Paleoproterozoic, carbon, oxygen, iron formation, microfossils
13

1. Introduction

When the Paleoproterozoic Era (2500-1600 million years ago; Ma) began, Earth's biosphere contained little free oxygen (Holland, 2006). By the time it ended, however, sulfidic water masses commonly lay beneath an oxygenated atmosphere and surface ocean (Canfield, 1998; Shen et al., 2002, 2003; Brocks et al., 2005; Scott et al., 2008). Accumulating evidence suggests that Paleoproterozoic environmental transition was episodic, with an initial influx of O₂ near the beginning of the interval followed nearer to its end by a resurgence of iron formation and subsequent long term loss of ferruginous deep waters (Poulton et al., 2004, Johnston et al. 2006). Available paleobiological data are consistent with hypothesized environmental changes. For example, distinctive microfossil assemblages of the type first reported from cherts of the Gunflint Formation, Canada (Barghoorn and Tyler, 1965, Cloud 1965), occur broadly in successions deposited after the initial rise of atmospheric oxygen and before the long term loss of ferruginous deep waters. To date, however, there have been only limited attempts to integrate paleobiological, biogeochemical, and environmental geochemical data within a tightly constrained framework of sequence stratigraphy and geochronology.

To better understand the relationship between evolving ocean chemistry and Paleoproterozoic life, we examined the Duck Creek Formation, a late Paleoproterozoic carbonate platform preserved in the Ashburton Basin of Western Australia. The Duck Creek succession contains more than 1000m of well preserved carbonate-dominated stratigraphy. Early mapping (e.g., Daniels, 1970) facilitated reconnaissance level studies of microfossils (Knoll and Barghoorn, 1976; Schopf, 1983; Knoll et al., 1988) and carbon isotopes (Schopf, 1983; Veizer et al., 1992a; Lindsay and Brasier, 2002), as well as detailed investigations of stromatolites (Walter 1972; Grey 1985; Grey and Thorne, 1985) and sequence stratigraphy (Thorne, 1983; Grey and Thorne, 1985) through at least part of the succession. Moreover, SHRIMP U-Pb dates for zircons in intercalated volcanic rocks now constrain depositional ages for Duck Creek and succeeding Ashburton strata (see below). This study documents sequence development for the entire Duck Creek succession and uses this framework to interpret carbon and oxygen isotopes at high

1 stratigraphic resolution, in addition to mineralogical and paleobiological data from the
2 same samples.

3 4 **2. Geologic Setting**

5
6 In the northwestern corner of Western Australia, Paleoproterozoic sediments are
7 preserved in the Ashburton Basin, a 12 km package of siliciclastics, carbonates,
8 volcanics, and iron formation distributed over 30,000 km² (Figure 1). Accommodation
9 space resulted from crustal loading associated with collision of the Pilbara and Yilgarn
10 cratons during the Capricorn Orogeny, creating the Ashburton foreland (Thorne and
11 Seymour, 1991). The Paleoproterozoic Wyloo Group lies disconformably above
12 modestly to moderately metamorphosed iron formations, carbonates and other lithologies
13 of the Neoarchean-Paleoproterozoic Mount Bruce Supergroup. The Wyloo Group
14 contains two carbonate platforms capped by volcanics and a thick siliciclastic succession,
15 and was itself deformed during subsequent Capricorn events, with the metamorphic grade
16 increasing toward the south. Because deformation is basically limited to thin-skinned
17 folding and thrusting, the degree of structural rotation is, in most places, low (30-40°),
18 and overlying Ashburton Formation mudstones and iron formation have experienced only
19 sub-greenschist metamorphism. This is in contrast with the rocks of the Earraheedy
20 Group to the southeast, deposited on the southern margin of the orogen (Halilovic et al.,
21 2004; Jones et al., 2000).

22 Though clearly present throughout the fold-and-thrust belt (and visible from air
23 and satellite photos), outcrops of the middle Wyloo Group, including siliciclastic and
24 carbonate sediments of the Mount McGrath Formation and Duck Creek Dolomite, are
25 discontinuously exposed. However, just north of Wyloo Dome in the heart of the Duck
26 Creek Syncline, Duck Creek Gorge offers near continuous exposure of the Duck Creek
27 Formation on both sides of the drainage; this is the location of data presented here. Near
28 Paraburdoo, farther to the southeast along the outcrop belt, another nearly complete Duck
29 Creek Formation section is exposed. The formation is thinner there and appears to
30 contain a slightly different facies succession (Thorne 1983).

At Duck Creek Gorge (22°29'00"S, 116°19'10"E), carbonates cover a 4.5 km transect as exposed in map view; over approximately half of that distance, vegetation and alluvium prevent identification of bedrock (Figure 1). Within the gorge, basal Duck Creek dolomites lie conformably above siltstones of the Mount McGrath Formation. To the north of Duck Creek Gorge, the Duck Creek succession is overlain conformably by basalt and tuffs of the June Hill Volcanics, whereas the southwestern portion of the dolomite in the core of the Duck Creek Syncline is capped by the highly cleaved and foliated fine-grained siliciclastics and iron formation of the Ashburton Formation. The onset of Duck Creek sedimentation is constrained by a 2209 ± 15 Ma SHRIMP U-Pb date on the Cheela Springs Basalt, found lower in the Wyloo succession (Martin et al., 1998). Its end is constrained by a series of ca. 1800 Ma SHRIMP U-Pb ages on June Hill volcanic rocks, including a new U-Pb SHRIMP date on a tuff approximately 5 km northwest of the study site, reported here (Nelson, 2003; Sircombe, 2003; Evans et al., 2003; see below). From the points of view of sedimentary patterns and basin analysis, the age of the Duck Creek Formation lies relatively close to the minimum age constraint provided by overlying June Hill tuffs (discussed below).

3. Methods

Rock samples were sectioned using a diamond saw and micro-drilled following methods of Kaufman (1990) to obtain fresh powders. Carbonate $\delta^{13}\text{C}$ and $\delta^{18}\text{O}$ values for 418 samples were measured concurrently on a VG Optima dual inlet mass spectrometer fed by an Isocarb preparation device in the Harvard University Laboratory for Geochemical Oceanography. Carbonate samples (~1 mg) were dissolved in a common anhydrous phosphoric acid (H_3PO_4) bath kept at 90°C for 8 minutes. Carbon dioxide gas was purified cryogenically and subsequently measured against an in-house reference gas (CO_2). Analytical uncertainty was $\pm 0.1\text{‰}$ (sample:standard ratio of 8:1); results are reported on a Vienna Pee Dee Belemnite scale.

Mineralogical composition was measured for 18 samples distributed throughout the formation. Constituent minerals were characterized by X-ray diffraction (XRD) with a Scintag, Inc. XDS 2000 diffractometer, using $\text{Cu K}\alpha_1$ radiation at 40 kV and 30 mA

1 according to methods described by Tosca et al. (2004). For all samples, data were
2 collected at 0.02° 2 θ steps, between 5° and 65° 2 θ . Peak matching of XRD patterns was
3 done using Crystallographica Search-Match®, an iterative phase identification program
4 used for multiphase powder diffraction patterns. Multiphase patterns were matched
5 against the Powder Diffraction File with restrictions on phase chemistry that limited
6 searches to minerals containing common rock-forming elements (H, C, O, Na, Mg, Al,
7 Si, P, S, Cl, K, Ca, Mn, or Fe). Phases with best fits were removed from the spectrum
8 and the search was iterated for less-abundant phases. Mineral abundances were
9 quantified using XRD data and the publicly available RockJock spreadsheet (maintained
10 by the USGS and available at <ftp://brrcrftp.cr.usgs.gov/pub/ddeberl>). RockJock matches
11 measured XRD peaks to a database of mineral XRD peaks in order to quantify percent
12 abundances. Measured peaks were matched against a database of 22 carbonates and
13 rock-forming minerals and 17 clay minerals. In order to identify any expandable clays
14 that may have been present, a sample of the clay fraction from mid-Duck Creek iron
15 formation was saturated in ethylene glycol.

16 Zircons were separated from a tuffaceous ash bed within the overlying June Hill
17 Volcanics (Figure 1C) using conventional heavy liquid and magnetic techniques followed
18 by hand-picking by MinSep Laboratories, and mounted in epoxy with the BR266 zircon
19 reference standard (206Pb/238U age of 559 Ma and 903 ppm U). The epoxy mount was
20 polished to expose grain cores in section, imaged using a scanning electron microscope
21 and gold coated prior to SHRIMP (sensitive high resolution ion microprobe) analysis.
22 The SHRIMP analytical procedures follow Compston et al. (1984) and Smith et al.
23 (1998).

24 25 26 **4. Duck Creek Sequence Stratigraphy**

27
28 Thorne (1983; see also Grey and Thorne, 1985) provided detailed
29 sedimentological and sequence stratigraphic interpretation of a 220 m section of the
30 lower Duck Creek Formation prominently exposed in a canyon wall at Duck Creek
31 Gorge. This work builds on that framework and extends it to cover the entire Duck

Creek stratigraphy. In addition to the peritidal to shallow subtidal facies recognized by Thorne (1983), major developments of subtidal stromatolitic bioherms, mound-and-channel systems, deeper-water limestones interbedded with dolomitic turbidites, and iron formation are present. These observations allow definition of the full suite of system tracts within the Duck Creek sequences, with the result that a broader range of paleowater depths can be reconstructed.

The Duck Creek Formation contains one complete depositional sequence, and parts of two others; the base of the formation is marked by the highstand of an underlying sequence, and the top of the formation is marked by the transgressive system tract of an overlying sequence. This formation-capping transgressive system tract defines the terminal drowning of the Duck Creek carbonate platform. The Duck Creek sequences are defined on the basis of a single measured section, shown in Figure 2.

4.1. Sequence 1

Highstand System Tract [0-142 meters]. The lower part of the Duck Creek Formation comprises the upper, shallowing part of a highstand system tract. Lithostratigraphically, the highstand is first recorded by the conformable contact with the underlying Mount McGrath Formation, exposed at the eastern edge of Duck Creek Gorge. Across this contact, black, tabular-bedded (~10 cm beds) Mount McGrath siltstones grade upward into a fine-grained, white siltstone, capped in turn by hummocky- and swaly-cross-stratified dolomite. Within the dolomite, large-amplitude (>20 cm) symmetric ripples, teepee structures, and imbricate flat-pebble conglomerates occur, along with late diagenetic cherts. The lowermost 40m, from the Mount McGrath contact, is the only part of the Duck Creek Formation that exhibits sedimentary structures other than stromatolites.

The presence of hummocky cross-stratification (HCS), as well as sedimentary structures that include rip-ups, wave ripples, teepee structures and imbricate flat-pebble conglomerates, indicates a moderate- to high-energy outer shoreface environment. HCS is commonly associated with deposition above storm wave base (Einsele, 2000). Imbricate clasts are more characteristic of storm-dominated, shallow-water environments

near or within the intertidal zone. Overall, the lower 38 m (section G, Figure 2) is interpreted as a shallow marine dolostone, punctuated by deepening (as recorded by HCS) to storm wave base.

These shallow water dolostones grade upward into ~100 m of m-scale parasequences characterized by imbricated flat-pebble conglomerates, teepee structures, and mitten-shaped stromatolitic precipitates. These peritidal facies mark the top of the highstand system tract. The boundary between Sequence 1 and Sequence 2 is not associated with karst or other evidence of subaerial exposure. Consequently, it is likely that subsidence rates were sufficiently high to prevent long-term exposure.

4.2 Sequence 2

Sequence 2 is the only identified stratigraphic sequence contained entirely within the lithostratigraphically-defined Duck Creek Formation.

Transgressive System Tract [142-258m]. The transgressive system tract of Sequence 2 is marked by grainstones that are intercalated with three m-scale bioherms (at 150-152 m, 163-164 m, and 232-238 m), composed of close-packed, columnar stromatolites. In plan view, the bioherms consist of circular- to elliptical columns with regular mm-scale laminae and well-defined intercolumnar spacing, usually 1.1 ± 0.2 cm. Mound-and-channel facies are present, as well, at 212-224 m and 224-232 m in the measured section. The channel fills contain thin lenses of wrinkled, low-relief (<2 cm), heavily silicified stromatiform precipitates. Locally, stromatolite initiation is marked by tungussiform shapes that grade upward into vertical columns (Figure 3D).

Maximum Flooding Interval [258-260m]. The uppermost bioherm is capped by a thin iron formation at 258 m that represents a maximum flooding interval. This ~1m thick bed is the lower of two iron formations identified within the Duck Creek Formation. (A third iron formation unit occurs in overlying beds of the lower Ashburton Formation.) Hematite grains and dark blue early diagenetic chert nodules containing rare detrital pyrite grains occur in two discrete layers within the Fe-rich unit. Indeed, while late diagenetic silica is widely distributed in Duck Creek carbonates, early diagenetic (pre-

compaction) chert nodules occur only in the deeper facies that also host iron formation. Above the iron formation, ~10 cm thick beds of imbricate flat-pebble conglomerate occur within fine- to coarsely-laminated beds. These beds alternate on the meter scale with domal, silicified dolomite precipitates.

Highstand System Tract [260 – 440m]: This is the Duck Creek interval investigated by Grey and Thorne (1985). The first ~ 200 m above the MFI iron formation represent shallowing to peritidal water depths and the formation of repetitive, stacked peritidal parasequences (Figures 3, 4). Here 1 to 1.5 m parasequences of shallow-water carbonates initiate with stromatolites of low synoptic relief draped by dolomitic laminites, with locally extensive development of sub-cm-scale microdigitate, precipitated stromatolites. Within this interval, parasequences are commonly capped by beachrock that records sea level shallowing to exposure. Precipitated stromatolites include domal structures up to 0.5 m high, laterally-linked conical structures with 3-4 cm of synoptic relief, and fan-shaped domes truncated by flat-pebble conglomerates. Precipitated stromatolite parasequences are topped by a massive dolomitic grainstone. No chert nodules were found in association with the precipitate units, but diffuse, late diagenetic silicification is extensive. Under polarized light, precipitates contain rhomboidal dolomite crystals with minimal bed-to-bed variability, only trace amounts of organic matter, and some iron staining. Lamination is visible in hand-samples, but not in thin section.

In agreement with previous investigators (Thorne, 1983; Grey and Thorne, 1985; Lindsay and Brasier, 2002), the repeated pattern of low relief stromatolites truncated by beach rock is interpreted to record inter- to supratidal deposition along the margin of a carbonate ramp. Grainstones are rare, but truncation surfaces that record subaerial exposure are common. It is possible that the uppermost of these exposed, peritidal parasequences represents the boundary between Sequence 2 and Sequence 3. Similar to what was observed at the top of Sequence 1, this boundary is not marked by a single complex exposure surface. Instead, it appears that accommodation was substantial enough to allow deposition throughout this time interval, making the distinction between highstand and lowstand systems tracts difficult without further study of parasequence stacking trends.

4.3 Sequence 3

Transgressive System Tract [440-640m]. The peritidal strata of the Sequence 2 Highstand are overlain by massive dolomitic grainstones interbedded with occasional <1 meter beds of columnar stromatolites. These grainstones constitute the transgressive system tract of Sequence 3. The grainstones grade upward into a ~20 m thick stromatolitic bioherm composed of columnar stromatolites with regular and well-defined intercolumnar spacing. And, like the Sequence 2 bioherms, this biohermal unit is succeeded by a gradual transition to iron formation marking the further flooding and backstepping of the platform to greater water depths.

Maximum Flooding Interval [640-660m]. The Sequence 3 maximum flooding interval is distinctive in containing a significant iron formation, approximately 20 m thick. This iron formation unit contains abundant early diagenetic chert and carbonate nodules, in contrast to the much thinner iron formation in the MFI of Sequence 2. Carbonates containing increasing abundances of potassium feldspars and hematite grade into thin-bedded to laminated iron formation containing carbonate- and silica-rich phases. Buff-weathering carbonate-rich beds alternate with hematite-rich beds near the base of the iron formation, but bedded carbonates decrease in abundance through the ironstone. In thin section, carbonates within the iron formation unit consist mostly of iron-stained ankerite euhedra. The iron formation grades upward into a more carbonate-rich, white- to brown-weathering unit composed of subangular iron-stained quartz grains mixed with rhombohedral carbonate crystals. This, in turn, is capped by a minor further development of hematitic ironstone and buff-weathering dolomite, similar to those found below the carbonate.

Unfortunately, the iron formation is followed by ~ 100 m of cover where Duck Creek takes a jog along strike, possibly as the result of a fault (Fig. 1c, indicated by dashed line). Where outcrop resumes, the strata consist of monotonous, buff-weathered, thickly-laminated dolostones (rhythmites) with fossiliferous early diagenetic chert nodules and soft-sediment deformation structures (most commonly dm-scale slumps and

convolute bedding). These facies contain well-developed interbeds of tabular-clast, matrix-supported breccias. Breccia clasts are derived from facies equivalents of the interbedded rhythmites. This facies association is classically known from deeper-water carbonate slope environments (Grotzinger, 1986).

It is possible the Sequence 3 MFI iron formation is immediately overlain by shallower-water carbonate facies (not exposed), thus forming a highstand to Sequence 3. However, the simplest interpretation of the covered interval is that it represents resumption of carbonate production on the Duck Creek platform, but with transport into deeper water environments. In this case it could still be a highstand deposit – albeit a positionally down-dip, deeper water facies. Regardless, this covered interval contains the transition to deeper water facies marking the onset of terminal flooding and drowning of the Duck Creek platform.

Above the iron formation is a 40 meter slumped interval captured in section F, overlapping the intact stratigraphy captured in section C. This slumped unit has discrete margins that can be traced around the outcrop. It contains convolute bedding, and abundant breccia, composed of imbricate, tabular buff-weathering dolomitic clasts up to 20 cm thick, set in a dark, rust-weathering carbonate matrix. This coarser breccia deposit is provisionally interpreted as a slump facies (Figure 5). Where preserved, bed orientation is discordant to the regular strike of the beds in the principal section. In this section, lower beds of this unit contain abundant and localized iron staining. Given the anomalous isotopic compositions found within the off-section breccia; this unit is discussed in more detail below.

[660-1000m]: Continuing upward in our primary section (from 860 to 942 m), ferruginous limestone rhythmites are interbedded with dolomitic turbidites, displaying well-defined Bouma sequences (Figure 5). Dolomitic turbidites occur approximately every nine meters. Limestones are heavily silicified and pervasively stylolitized, and contain dolomite nodules that are oblate to bedding and exhibit differential compaction. The limestones commonly contain stylolites, often marked by high concentrations of iron minerals. In this section, limestones contain calcite crystals with small amounts of hematitic coating, but the majority of iron is concentrated within stylolites, suggesting that the limestones contained substantial amounts of iron at the time of stylolite

development. The presence of rhythmites and dolomitic turbidites, together with the absence of wave-influenced sedimentary structures, suggests deposition in an iron-rich environment well below wave-base and punctuated by turbidity currents. Near the top of the unit, two ~1 meter thick beds of black, highly cleaved siltstone presage a change in sedimentary regime, and following another ~150 m of cover the iron-rich, highly cleaved siltstones of the Ashburton Formation begin.

In summary, the 1000m Duck Creek Formation preserves a sequence stratigraphic architecture similar to that of other late Paleoproterozoic carbonate platforms (e.g., Grotzinger, 1986, 1989; Grotzinger and James, 2000): multiple sequences that grade upward from shallow subtidal grainstones and stromatolitic bioherms to peritidal carbonates with conspicuous precipitated microdigitate stromatolites. Maximum flooding intervals contain iron formation and other authigenic carbonate/silicate precipitates (see below), and slope/basinal facies are marked by (dolo)micrite and limestone rhythmites, rhythmite breccias, block breccias, and carbonate turbidites. Based on the presence of turbidites and slump features distal to peri- to supratidal precipitates, the overall platform architecture is that of a distally-steepened carbonate ramp. The repetitive sequence architecture enables us to differentiate between geochemical and paleobiological patterns that reflect environment and those recording secular change in a late Paleoproterozoic ocean.

4. Mineralogy and Geochemistry

4.1 Mineralogical clues to paleoenvironmental history

The Duck Creek Formation has long been characterized as dolomitic, with almost no development of siliciclastic lithologies. X-ray diffraction (XRD) data, however, shows that many Duck Creek carbonates are distinctly more iron-rich than this would suggest. In peritidal and shallow subtidal facies, sampled carbonates are predominantly ferroan dolomite $[\text{Fe,Mg}(\text{CO}_3)_2]$ and Mg- and Mn-rich ankerite $[\text{Ca}(\text{Mg}_{0.27}\text{Fe}_{0.66}\text{Mn}_{0.05})(\text{CO}_3)_2]$ (Figure 3, Table 1), with lesser amounts (<10%) of dolomite, quartz (as diffuse diagenetic silica), and, locally, clay minerals. Samples

associated with iron formation are distinctly different. Carbonate in these samples ranges from a few to about 70% by weight, with dolomite, ankerite, and calcite in approximately equal proportions. The iron formations contain up to 15% hematite and magnetite, as well as chert (i.e. microcrystalline quartz) abundances much higher than those of other facies. Clays and potassium feldspars, both authigenic, also reach their greatest abundances in this facies. These potassium feldspars are probably diagenetic products of preexisting zeolites and clays (Bish and Guthrie, 1993) based on their absence from hand samples and petrographic thin sections. The lack of visible evidence for feldspars, but their presence in XRD spectra, suggests that these minerals consist of small grains, which would be expected from alteration of preexisting clay minerals. Deep water carbonates in the upper part of the section differ again, consistently predominantly of calcite.

Silica and iron are closely correlated in Archean and Paleoproterozoic iron formations (see Fischer and Knoll, 2009, for recent discussion), and in the Duck Creek Formation, they covary on a sub-cm as well as outcrop scale. Throughout the formation, siderite (FeCO_3) is present only in low abundances (<5%); this is not surprising given the tendency of siderite to become dolomitized to ankerite (Klein and Beukes, 1989; Han 1978) or to decompose to magnetite (Fe_3O_4 ; Yui 1966) during burial diagenesis. Although rare pyrite grains were observed in thin sections of early diagenetic chert nodules, sulfide minerals are absent from bulk diffraction patterns throughout our sample set.

Clay minerals occur as minor components of most samples, but comprise up to 20% of iron formation lithologies. Iron formation samples show XRD peaks at 6.4, 12.5, and 26.6° 2 θ , indicating the presence of chlorite, berthierine, and 1M illite, respectively (Figure 3b). Glauconite is also found in lithologies associated with Duck Creek iron formation, and, in a glycolated sample, a small break in slope at 2.54° suggests minor occurrence of chaotically ordered expandable clay precursors, possibly smectite.

Berthierine $[(\text{Fe},\text{Al})_3(\text{Si},\text{Al})_2\text{O}_5(\text{OH})_4]$ and glauconite $[\text{K}(\text{Al},\text{Fe},\text{Mg})_2(\text{Si},\text{Al})_4\text{O}_{10}(\text{OH})_2]$ are particularly informative about Duck Creek environments. These iron-rich, aluminum-poor clay minerals form in marine environments at or near the sediment-water interface, in the presence of reduced iron and commonly associated with organic matter. Glauconite precipitates slowly, commonly

1 under low rates of sedimentation which allow potassium to diffuse from the overlying
2 marine water column into its structure during formation (Meunier, 2005). Today,
3 glauconite typically forms below the thermocline, at water depths of 125 - 250m (10-
4 15°C). Berthierine typically occurs in nearshore settings associated with relatively warm
5 temperatures (for favorable precipitation kinetics), corresponding to 10-50m water depth
6 (25-27°C) in the modern ocean, above the thermocline.

7 The Duck Creek succession records this slight separation, as berthierine peaks at
8 ~642 meters, within the carbonate-rich ironstones, whereas glauconite peaks within the
9 iron formation at approximately 658 m and is present in the deeper water limestones.
10 Because both berthierine and glauconite form through redox reactions near the sediment-
11 water interface, rather than through metasomatism, they corroborate the evidence of Fe-
12 rich carbonates in indicating an iron-rich marine setting. 1M-illite in Duck Creek
13 samples probably reflects the diagenetic transformation of original smectite clays.
14 Chlorite also occurs, but this mineral is typically the product of moderate metamorphism.

15 Heavily silicified samples from the lower part of the formation contain up to 7%
16 goethite. Like the possible smectite noted above, goethite in this section may have
17 originated relatively recently due to recent surface weathering. Goethite also provides a
18 fingerprint for zones of secondary alteration, and a possible indicator of areas where iron
19 minerals may be present due to present-day weathering elsewhere on the Pilbara Craton.
20 In the absence of core material, stratigraphic correlation between hematite and goethite
21 provides the most direct test of whether iron minerals formed from secondary alteration.
22 As noted above, hematite and other iron minerals reach their peak abundance within the
23 iron formation, rather than in the lower samples that have the highest concentrations of
24 goethite; this suggests at least some of the hematite in the iron formation is depositional.
25 That being said, it is clear from observations and hand samples that the entire
26 sedimentary sequence has been influenced by multiple episodes of diagenesis, most
27 obviously silicification.

28 In short, while iron formation provides the most obvious lithological
29 manifestation of ferruginous bottom-water conditions, both carbonate and clay
30 mineralogy indicate that the Duck Creek basin was iron-rich throughout the interval
31 recorded by our section. In coastal environments, continental run-off probably supplied

1 iron in oxidized form, which was reduced to Fe^{2+} within accumulating carbonates and
 2 incorporated into Fe-dolomite and ankerite by dolomitizing fluids. Basinal iron
 3 formations and associated Fe-carbonates more likely contain iron introduced from anoxic
 4 deep waters.

5 That carbonates deposited during maximum flooding remain calcitic may
 6 principally reflect the fact that basinal carbonates in the Duck Creek succession were
 7 emplaced mechanically, transported from shallower sites of precipitation. Ferrous iron
 8 would have been generated within anoxic deep waters and pore waters, but in the absence
 9 of dolomitization -- known to be less prevalent in basinal environments (e.g., Grotzinger,
 10 1989; Knoll and Swett, 1990) -- it was not readily incorporated into accumulating
 11 carbonates.

12 13 *4.2 Carbon Isotopes*

15 High resolution carbon isotope data for the Duck Creek carbonates display a wide
 16 range of variability, from -8.08 and +1.94‰, substantially greater than that reported by
 17 earlier workers (Veizer et al., 1992b; Lindsay and Brasier, 2002). Despite the broad
 18 overall range, however, a strong majority of measured values fall between +1.0 and -
 19 0.5‰. The shallowest carbonates displaying precipitated textures exhibit the most
 20 positive $\delta^{13}\text{C}$ values, averaging nearly 1‰, in contrast to subtidal stromatolites that
 21 average 0‰. Similarly modest ^{13}C -enrichment of peritidal carbonates has previously
 22 been recorded from Paleo- and Mesoproterozoic carbonates in other basins (e.g., Burdett
 23 et al., 1990; Knoll et al., 1995; Hotinski et al., 2004). The Duck Creek succession
 24 preserves carbonates deposited across a depth gradient likely to have exceeded 100 m,
 25 but there is no further ^{13}C -depletion recorded in basinal limestones and dolomites. As
 26 noted above, at least some deep water Duck Creek carbonates (breccias and turbidites)
 27 reflect basinward transport of carbonates precipitated in shallower water. However, for
 28 finer-grained facies this must be inferred.

29 That noted, the most negative $\delta^{13}\text{C}$ values in the Duck Creek succession do occur
 30 in maximum flooding intervals within the succession, clustered into three sharp
 31 excursions (Figure 2; see Table 1). Two of these are closely tied to the iron formations

developed in each major sequence; the third is contained within the megabreccia appearing at 820-828 m in the upper part of the section (i.e. Section F).

A number of studies have reported large differences in carbonate carbon isotope composition of shallow-water dolomitic carbonates ($\delta^{13}\text{C} \sim 0\text{‰}$) and coeval carbonates associated with basinal iron formation ($\delta^{13}\text{C} \sim -5$ to -7‰) (e.g., Becker and Clayton, 1972; Beukes and Klein, 1990; Beukes et al., 1990; Kaufman et al., 1990). To explain this gradient, conventional models invoke a stronger biological pump and a globally stratified ocean capable of producing and maintaining a carbon isotope depth gradient (Derry et al., 1992; Given and Lohmann, 1985; Hotinski et al., 2004; Kaufman et al., 1990; Kennedy, 1996; Surge et al., 1997). However, careful analysis of seafloor carbonate precipitates deposited along a depth gradient in the late Paleoproterozoic Pethei Group, Canada, detected no strong C-isotopic variation with depth (Hotinski et al., 2004). More recently, detailed C-isotopic investigation of carbonates deposited along the margin of the Neoproterozoic Campbellrand-Kuruman platform not only corroborated the absence of a discernable C-isotopic depth gradient in seafloor precipitates formed across a paleodepth range of several hundred meters, but also showed that siderites in basinal iron formation differ from sub- and suprajacent CaCO_3 precipitates in recording variable, but commonly strong ^{13}C -depletion (Fischer et al., 2009).

Such observations suggest that the ^{13}C depletion observed in iron formation carbonates must reflect processes other than a hyperactive biological carbon pump. Fischer et al. (2009) proposed that carbon isotope depletion associated with siderite, a carbonate mineral often associated with iron formation, reflected complex interactions among iron oxide minerals, soluble silica, and iron-reducing bacteria. In this model, complexes of iron oxides and adsorbed silica were transported from surface waters to the deep seafloor, where anaerobically respiring bacteria used the ferric iron as a terminal electron acceptor. This resulted in the precipitation of mixed valence and reduced iron minerals, including siderite.

Iron respiration is a heterotrophic process, oxidizing organic matter back to carbon dioxide. Five analyses of organic carbon in Duck Creek carbonates yielded $\delta^{13}\text{C}$ values of ca. -25‰ ; a single measurement of organic carbon in a Duck Creek chert yielded a value of -31.7‰ (Schopf, 1983). Such fractionation is typical of ecosystems

1 fueled by RUBISCO-based autotrophy (House et al., 2000; Robinson and Cavanaugh,
 2 1995). The depleted $\delta^{13}\text{C}$ signature from the oxidized or respired organics can contribute
 3 to the dissolved inorganic carbon pool that feeds local precipitation of carbonate. Thus,
 4 accumulating carbonates can contain markedly depleted $\delta^{13}\text{C}$ values, similar to those
 5 observed in the Duck Creek Formation. Simple mass-balance would suggest that in the
 6 most extreme of cases (-8‰; 658 m), 25-33% of the carbonate carbon came from
 7 remineralized organic matter. The general expectation is that carbonates precipitated on
 8 or within the seafloor in association with iron oxide minerals should record more
 9 depleted $\delta^{13}\text{C}$ values than overlying or underlying iron oxide-poor facies. This is exactly
 10 what is observed within the Duck Creek, and as such, provides a reasonable interpretation
 11 for the lower two negative carbon isotope events.

12 As noted above, the uppermost negative carbon isotope anomaly is not associated
 13 with iron formation. Carbonate minerals in this horizon are similar to those found in
 14 shallow-water facies, comprising dolomite, ankerite, and Fe-dolomite. This unit contains
 15 very little calcite and even less quartz, unlike other deeper-water samples above the iron
 16 formation. Certain samples, however (specifically F0 and F6; Table 1), exhibit
 17 significant iron staining on carbonate grains (Plate 3). This staining suggests that pore
 18 fluid iron played a role in the diagenetic environment of these highly permeable breccias.
 19 Percolating fluids could have supported a similar microbial iron-cycling community to
 20 that found in association with the iron formation, resulting in a similar $\delta^{13}\text{C}$ signal.

21 22 4.3. The $\delta^{18}\text{O}$ record

23
 24 Oxygen isotope ratios ($\delta^{18}\text{O}$) in ancient carbonates can provide a measure of post-
 25 depositional water-rock interaction. Given that a vast majority of Precambrian
 26 carbonates have been recrystallized, and secondary fluids are rich in O (from water), but
 27 poor in C, the oxygen isotope composition of carbonates is differentially vulnerable to re-
 28 setting. The result is that carbonates commonly acquire a $\delta^{18}\text{O}$ composition similar to
 29 that of diagenetic waters, which commonly deviate from $\delta^{18}\text{O}$ composition of seawater
 30 (Veizer et al., 1992a, 1992b). Although this classic interpretation has been challenged by
 31 recent work exploring carbonate diagenesis through the lens of clumped isotope

1 paleothermometry, suggesting that diagenetic alteration can either enrich (via high-
 2 temperature fluids) or deplete (via meteoric water) carbonates in ^{18}O (Came et al., 2007),
 3 the simple claim that the $\delta^{18}\text{O}$ of carbonate is susceptible to alteration holds. This is our
 4 point of entrance to the interpretation of Duck Creek $\delta^{18}\text{O}$ chemostratigraphy.

5 $\delta^{18}\text{O}$ values of the Duck Creek carbonates range from -14 to +5‰ VPDB (Figure
 6 2). Perhaps surprisingly, O-isotopes show strong bathymetric coherence; shallow water
 7 sections are relatively enriched in ^{18}O (~0 to 4‰; mean = 0.8‰), whereas deeper water
 8 sections, including iron formation carbonates, are commonly more ^{18}O -depleted (mostly -
 9 6 to +3‰; mean = -4.5‰). It has been suggested that a common mode of isotopic
 10 behavior during diagenesis leads to covariation of carbon and oxygen isotope ratios
 11 (Knauth and Kennedy 2009). In the Duck Creek Formation sections, $\delta^{13}\text{C}$ and $\delta^{18}\text{O}$
 12 values do not covary, either through the section as a whole (Figure 8a) or within the
 13 section at 600 to 700 meters, an interval marked by successive ^{13}C -depleted samples in
 14 iron formation and ^{18}O -depletion in underlying carbonates (Figure 8b). The ^{18}O -depleted
 15 carbonates contain carbon isotope values similar to shallow-water carbonates throughout
 16 the section; ^{13}C -depleted ironstone samples contain oxygen isotope values similar to
 17 intermediate to shallow carbonates throughout the section. The heaviest $\delta^{18}\text{O}$ values
 18 recorded in our sample set occur in the megabreccia unit described earlier; comparable
 19 $\delta^{18}\text{O}$ values have been interpreted as reflecting late-stage alteration by basinal fluids at
 20 relatively elevated temperatures (50-70°C) (Came et al. 2007).

21 The pronounced stratigraphic pattern recorded by Duck Creek carbonates reflects
 22 the relative timing of cementation, dolomitization and recrystallization processes that
 23 collectively determine the extent to which sediments can interact with diagenetic fluids.
 24 In peritidal environments, rapid cementation and penecontemporaneous dolomitization
 25 commonly preserved least-altered stable isotopic signals (Burdett et al., 1990). In deeper
 26 subtidal settings, however, cementation and dolomitization commonly occur later, if at
 27 all, allowing calcium carbonate minerals to recrystallize in continuing contact with
 28 diagenetic fluids depleted in ^{18}O (Burdett et al., 1990, Schidlowski et al., 1983,
 29 Zempolich et al., 1988).

30 Like many Precambrian carbonates, petrographic examination of Duck Creek thin
 31 sections suggests wholesale recrystallization. This is supported by the widely variable

oxygen isotope composition seen in the dataset. The stratigraphic pattern shows a repeating monotonic trend through two deepening-upward cycles—specifically, small first differences in $\delta^{18}\text{O}$ between stratigraphically contiguous samples. Shallow water samples are typically enriched in ^{18}O (~2‰), whereas deep-water samples are ^{18}O -depleted (-6‰). There is a general, but not one-to-one, correlation between percent calcite and ^{18}O -enrichment, suggesting that oxygen isotope variation is controlled by the vulnerability of calcite (compared to dolomite) to alteration during burial diagenesis. Deeper-water sediments (e.g., limestones from sections D and E) have a higher proportion of calcite and were cemented later (made clear from the differentially compacted dolomite nodules in limestone matrix). Because mineralogy is a function of depth, this gives the illusion of a depth gradient in oxygen isotope composition.

4.4 Geochronology

Zircon morphology: The morphology of zircons separated from sample JVT includes typical tuffaceous sizes and shapes: i.e. 30-100 microns in size, aspect ratio typically 1.5-2.0 with fine concentric euhedral internal zoning and euhedral to subhedral external morphology. Several such grains show evidence of abrasion with chipped external surfaces which crosscuts the internal euhedral zoning visible on cathodoluminescence (CL) images. A minority of zircon grains are fragments of larger grains, and also have the 30-100 micron size range and 1.5-2.0 aspect ratio.

Age of the June Hill Volcanics: The U-Pb isotopic data for the June Hill Tuff sample are presented in Table 3. The $^{207}\text{Pb}/^{206}\text{Pb}$ age data shows considerable scatter and reflects a complex zircon inventory in the tuffaceous sample. There is one dominant age population (11 of 24 analyses <10% discordant) which comes exclusively from finely zoned, euhedral to subhedral zircons typical of magmatic growth. All except one of these analyses are $\leq 3\%$ discordant (Table x) and they represent a single statistical age population (MSWD = 0.84) which yields a pooled $^{207}\text{Pb}/^{206}\text{Pb}$ age of 1795 ± 7 Ma (95% c.l.; Fig. 11). This age is within analytical error of other estimates of the June Hill Volcanics (discussed below) and given the zircon morphologies is considered to date the tuffaceous event.

Other zircons in the sample are both older and younger. Five of the six older zircons are within 1% of concordant and yield ages of 1834 to 3470 Ma (Appendix 3). These grains are mostly fragments of larger grains with the external surface crosscutting internal zonation in CL images. Most grains have rounded corners typical of detrital grains and together with similar, although less severe, textures in the magmatic population the tuff is interpreted to have been reworked. The age range of the older grains corresponds to components of the underlying stratigraphy and granitoids and is compatible with a hinterland of known Pilbara and Yilgarn Craton rocks at the time of tuffaceous volcanism.

The younger grains found in the sample range in age from 1765 to 1185 Ma (Appendix 3). All except one of these nine analyses are $\leq 2\%$ discordant, which is unusual if the normal explanations of diffusional Pb-loss and resetting are considered to explain ages younger than the rock formation age. The three oldest grains of this group (i.e. 1742-1765 Ma; Appendix 3) are morphologically similar to the 1795 Ma magmatic population and are interpreted to be part of this group and suffered minor diffusional Pb-loss prior to Recent times. Including these with the eleven magmatic analyses produces unacceptably high scatter in the population for a single age (i.e. MSWD = 1.8 for $n = 14$) and validates their omission from the magmatic group for the purposes of an age calculation.

The ages for the remaining six youngest analyses (Appendix 3) do not cluster to indicate a discrete resetting event, and are mostly outside the age range of known events to affect the rocks (e.g., the Capricorn Orogeny). Further, their shape and size are largely indistinguishable from the other zircons in the rock. Although not definitive, this suggests they were 1795 Ma or older zircon grains incorporated into the rock at its time of formation and thereafter lost Pb by diffusion to fortuitously remain close to concordant. Other explanations of partial resetting during unknown or poorly characterized events after 1795 Ma remain possible but cannot be tested without more extensive studies, which are outside the aim of determining the age of the tuffaceous volcanic event.

5. Micropaleontology

1 The modern era of Precambrian micropaleontology began with the discovery of
2 fossils in the ca. 1900 Ma Gunflint Formation, Canada (Tyler and Barghoorn, 1954;
3 Barghoorn and Tyler, 1965; Cloud 1965). Carbonaceous cherts associated with Gunflint
4 iron formation contain dense concentrations of microfossils, preserved as organic remains
5 or iron oxide replicas. Gunflint-like assemblages were subsequently recorded from other
6 late Paleoproterozoic iron formations, including the Sokomon Formation in Labrador,
7 Canada (Knoll and Simonson, 1981), and the Frere Formation, Australia (Walter et al.,
8 1976; Tobin, 1990). Gunflint-type assemblages differ markedly from the cyanobacterial
9 fossils found in silicified peritidal carbonates of comparable age from the Belcher
10 Islands, Canada (Hofmann, 1976; Golubic and Hofmann, 1976), suggesting that they may
11 record environmentally and/or metabolically distinct communities.

12 The sizes and shapes of Duck Creek microfossils are closely similar to those
13 found in Gunflint chert, including 1-2 μm filaments assigned to the genus *Gunflintia*,
14 small cocci assignable to *Huroniospora*, and asteriform microfossils placed within
15 *Eoastrion*, as well as rare larger trichomes comparable extant oscillatorian cyanobacteria
16 or sulfur-oxidizing bacteria (Knoll and Barghoorn, 1976; Knoll et al., 1988; Figure 9).
17 Microfossils in cherts collected within the measured section are similar to those reported
18 previously.

19 Early work on Duck Creek microfossil assemblages demonstrated their taxonomic
20 affinity to the Gunflint biota (Knoll and Barghoorn, 1976; Knoll et al., 1988) but lacked
21 the sequence stratigraphic context needed to facilitate environmental comparisons with
22 Canadian assemblages. Our stratigraphic investigation now provides a unique framework
23 to test the proposal (Knoll, 2003) that Gunflint-like biotas record iron-metabolizing
24 bacteria that lived close to the oxycline in ferruginous Paleoproterozoic oceans.

25 Early diagenetic silica provides an important taphonomic window on Proterozoic
26 life, and the processes that remove silica from seawater and redistribute it locally within
27 sediments to form nodules will strongly influence the types of communities seen through
28 this window. For much of Proterozoic time, silica left the oceans primarily as an early
29 stage evaporite, deposited along ocean margins (Maliva et al., 1989). For this reason,
30 peritidal mats rich in cyanobacteria are commonly found in early diagenetic cherts.
31 Adsorption on iron oxides, however, provides another means of removing silica from

1 seawater, and one that would have been important in Archean and Paleoproterozoic
2 basins where iron formation was deposited (Fischer and Knoll, 2009).

3 In the Duck Creek Formation, early diagenetic chert is essentially absent from
4 peritidal parts of the succession, but abundant in deeper facies associated with iron
5 formation. Not surprisingly, then, Duck Creek cherts contain no assemblages comparable
6 to that of the Belcher Islands, but abundant Gunflint-like fossils. Because peritidal
7 carbonates in the Duck Creek succession do not contain early diagenetic cherts, we
8 cannot be certain about microbial communities in that setting. That said, comparable
9 facies throughout the Proterozoic contain assemblages dominated by cyanobacteria and
10 cyanobacteria-like microfossils (Knoll 2003).

11 The presence of early diagenetic nodular cherts associated with iron deposition
12 suggests that the Duck Creek microbiota existed near (or slightly below) the sediment-
13 water interface, possibly close to a redoxcline. A redox interface would both provide a
14 chemical source of harvestable energy and ferrous iron for the iron formation. As early
15 as 1965, Cloud (1965) compared Gunflint filaments and asteriform microfossils with iron
16 bacteria found in modern ferruginous environments. Sequence stratigraphic
17 interpretation of Duck Creek microfossils supports such an interpretation and provides a
18 simple explanation for the apparent restriction of Gunflint-type assemblages to
19 Paleoproterozoic strata deposited after the initial rise of oxygen but before the demise of
20 Fe-rich deep waters (Knoll, 2003).

22 **6. Redox conditions in the Ashburton Basin**

24 More than a decade ago, Canfield (1998) proposed that the demise of
25 Paleoproterozoic iron formations resulted not from the expansion of oxygenated deep
26 waters but rather by the establishment of sulfidic chemistry in anoxic subsurface water
27 masses. In this hypothesis, the initial rise of oxygen in the atmosphere and surface ocean
28 resulted in an expanding sulfate reservoir. The presence of pyritic shales in latest
29 Paleoproterozoic rocks is hypothesized to represent an expansion of bacterial sulfate
30 reduction that resulted in the titration of ferrous iron from anoxic deep waters. The
31 global nature of redox conditions in late Paleoproterozoic deep waters remains uncertain,

1 although dysoxic, non-sulfidic water masses clearly existed (Slack et al., 2009). Water
2 masses immediately beneath the oxygenated mixed layer, however, were commonly
3 anoxic and sulfidic in latest Paleoproterozoic and Mesoproterozoic oceans (e.g., Shen et
4 al., 2002, 2003; Brocks et al., 2005; Scott et al., 2008).

5 In the late Paleoproterozoic Animike Basin of northwestern Ontario, hematitic
6 iron formation is overlain by sulfide-rich shales and siltstones. On the basis of Fe-
7 speciation studies, Poulton et al. (2004) proposed that this stratigraphic pattern captures
8 the transition from ferruginous to sulfidic subsurface waters, completed before ca. 1840
9 Ma. By itself, however, the Animike record cannot tell us (1) whether Paleoproterozoic
10 iron formations record the persistence or resurgence of Fe-rich deep waters, (2) whether
11 Paleoproterozoic ferruginous waters developed regionally or globally, or (3) whether the
12 transition to sulfidic subsurface waters occurred synchronously throughout the oceans.
13 Paleoproterozoic successions from Western Australia, including the Ashburton Basin,
14 provide perspective on these questions.

15 In Australia, iron formation occurs in a siliciclastic-dominated succession within
16 the Earraheedy Basin, on the conjugate side of the orogen associated with the Yilgarn
17 Craton (Halilovic et al., 2004). Commonly interpreted as correlative with Duck Creek
18 rocks, Earraheedy iron formation is constrained to be older than 1790-1760 Ma, the timing
19 of regional deformation (e.g., Halilovic et al., 2004). U-Pb SHRIMP dates on detrital
20 zircons in sandstones of the Yelma Formation deposited before the onset of iron
21 deposition indicate a depositional age younger than 1983 ± 51 Ma and 2032 ± 27 Ma;
22 detrital zircons in sandstones that overlie the iron formation include grains as young as
23 1808 ± 36 Ma (Halilovic et al., 2004).

24 As noted earlier, the age of the Duck Creek Dolomite is constrained U/Pb dates
25 on overlying June Hill Volcanics of 1806 ± 9 Ma (Nelson, 2003) and 1799 ± 8 Ma (Evans
26 et al., 2003). The new U-Pb date reported here is consistent with earlier determinations,
27 but is significant because the sampled ashbed lies directly on top of upper Duck Creek
28 Formation carbonates and below hematite iron formation of the overlying Ashburton
29 Formation in the same section (Thorne and Seymour, 1991). Thus, the 1795 ± 7 Ma age
30 reported here provides direct confirmation that ferruginous waters persisted in the

Ashburton foreland basin until ca. 1800 Ma or later, a minimum of tens of millions of years after they disappeared in North America.

7. Conclusions

The Paleoproterozoic Duck Creek carbonate platform developed in a basin characterized by ferruginous bottom waters. Stromatolites in tidal flat to shallow subtidal environments probably record benthic microbial communities fueled by cyanobacterial photosynthesis (Grey, 1985). Deeper in the basin, however, an oxycline existed, with moderately oxygenated waters above and anoxic ferruginous waters below. Near this interface, iron metabolism played a major role in microbial ecosystems, with chemotrophs and, possibly, phototrophs fixing carbon while iron-respiring bacteria returned carbon dioxide to the environment. Gunflint-type microfossils preserved in basinal Duck Creek cherts provide a fossil record of this community. The Duck Creek Formation testifies to the presence of distinctive Proterozoic ecosystems whose distribution in time and space waxed and waned with the distribution of iron-rich water masses beneath oxic surface oceans.

Acknowledgements. We thank the Agouron Institute for funding, Henry Goodall and Caroline Minnear for logistical support, Sally Sweetapple for field assistance, G. Eiseheid for mass spectrometry assistance, N. Tosca for XRD guidance, B. Croft for XRD support, R. Millikan and J. Creveling for thoughtful comments, and David Fike and one anonymous reviewer for constructive criticisms. JPW was supported in part by the NASA Astrobiology Institute.

References

- Amard, B., Bertrand-Sarfati, J., 1997. Microfossils in 2000 Ma old cherty stromatolites of the Franceville Group, Gabon. *Precambrian Research* 81, 197-221.
- Barghoorn, E.S., Tyler, S.A., 1965. Microorganisms from the Gunflint Chert. *Science* 147, 563-575.
- Becker, R.H., Clayton, R.N., 1972. Carbon isotopic evidence for the origin of a banded iron-formation in Western Australia. *Geochimica et Cosmochimica Acta* 36, 577-595.
- Bekker, A., Kaufman, A.J., 2007. Oxidative forcing of global climate change: A biogeochemical record across the oldest Paleoproterozoic ice age in North America. *Earth and Planetary Science Letters* 258, 486-499.
- Beukes, N.J., Klein, C., 1990. Geochemistry and sedimentology of a facies transition - from microbanded to granular iron-formation - in the Early Proterozoic Transvaal Supergroup, South-Africa. *Precambrian Research*, 47(1-2): 99-139.
- Beukes, N.J., Klein, C., Kaufman, A.J. and Hayes, J.M., 1990. Carbonate Petrography, Kerogen distribution, and carbon and oxygen isotope variations in an Early Proterozoic transition from limestone to iron-formation deposition, Transvaal Supergroup, South-Africa. *Economic Geology* 85, 663-690.
- Bish, D.L., Guthrie, G.D., 1993. Mineralogy of clay and zeolite dusts (exclusive of 1:1 layer silicates). *Reviews in Mineralogy* 28(1), 139-184.
- Brocks, J.J., Love, G.D., Summons, R.E., Knoll, A.H., Logan, G.A., Bowden, S., 2005. Biomarker evidence for green and purple sulfur bacteria in an intensely stratified Paleoproterozoic ocean. *Nature* 437, 866-870.
- Burdett, J.W., Grotzinger, J.P., and Arthur, M.A. 1990. Did major changes in the stable isotopic composition of Proterozoic seawater occur? *Geology*, v. 18, p. 227-230.
- Came, R.E. et al., 2007. Coupling of surface temperatures and atmospheric CO₂ concentrations during the Palaeozoic era. *Nature* 449, 198-201.
- Canfield, D.E. 1998. A new model for Proterozoic ocean chemistry. *Nature* 396, 450-453.
- Cloud, P.E., 1965. Significance of the Gunflint (Precambrian) microflora. *Science* 148, 28-35.
- Compston, W., Williams, I. S., Meyer, C., 1984. U-Pb geochronology of zircons from lunar breccia 73217 using a sensitive high mass-resolution ion microprobe. *Journal Geophysical Research*, 89, B525-534.
- Daniels, J.L., 1970. Explanatory notes:, Wyloo 1:250,000 geological sheet, Western Australia. Geological Survey of Western Australia, Perth, 20 p.
- Derry, L.A., Kaufman, A.J., Jacobsen, S.B., 1992. Sedimentary cycling and environmental change in the Late Proterozoic: Evidence from stable and radiogenic isotopes. *Geochimica et Cosmochimica Acta* 56, 1317-1329.
- Einsele, G., 2000. *Sedimentary Basins: Evolution, Facies, and Sediment Budget*. Springer-Verlag, Berlin.

- 1 Evans, D.A.D. et al., 2003. Revised geochronology of magmatism in the western
2 Capricorn Orogen at 1805-1785 Ma: diachroneity of the Pilbara-Yilgarn collision.
3 Australian Journal of Earth Sciences 50, 853-864.
- 4 Fischer, W.W., Knoll, A.H., 2009. An iron shuttle for deepwater silica in Late Archean
5 and early Paleoproterozoic iron formation. Geological Society of America
6 Bulletin 121, 222-235.
- 7
- 8 Fischer, W.W. et al., 2009. Isotopic constraints on the Late Archean carbon cycle from
9 the Transvaal Supergroup along the western margin of the Kaapvaal Craton, South
10 Africa. Precambrian Research, 169(1-4): 15-27.
- 11
- 12 Given, R.K., Lohmann, K.C., 1985. Derivation of the original isotopic composition of
13 Permian marine cements. Journal of Sedimentary Research 55, 430-439.
- 14 Golubic, S., Hofmann, H.J., 1976. Comparison of Holocene and mid-Precambrian
15 Entophysalidaceae (Cyanophyta) in stromatolitic algal mats: cell division and
16 degradation. Journal of Paleontology 50, 1074-1082.
- 17 Grey, K., 1985. Stromatolites in the Duck Creek Dolomite, Western Australia.
18 Geological Survey of Western Australia, Report 14, Professional Papers for 1983,
19 pp. 94-103.
- 20 Grey, K., Thorne, A.M., 1985. Biostratigraphic significance of stromatolites in upward
21 shallowing sequences of the Early Proterozoic Duck Creek Dolomite, Western
22 Australia. Precambrian Research 29, 183-206.
- 23 Grotzinger, J.P., 1986. cyclicity and paleoenvironmental dynamics: Rocknest platform,
24 northwest Canada. Geological Society of America Bulletin 97, 1208-1231.
- 25 Grotzinger, J.P., 1989. Construction of early Proterozoic (1.9 Ga) barrier reef complex,
26 Rocknest platform, Northwest Territories. Canadian Society of Petroleum
27 Geologists Memoir 13, 30-37.
- 28 Grotzinger, J.P., James, N.P., 2000. Precambrian carbonates: evolution of understanding
29 SEPM Special Publication 67, 3-20.
- 30 Halilovic, J., Cawood, P.A., Jones, J.A., Pirajno, F., Nemchin, A.A., 2004. Provenance of
31 the Earahedy Basin: implications for assembly of the Western Australian Craton.
32 Precambrian Research 128, 343-366.
- 33
- 34 Han, T.-M., 1978, Microstructures of magnetite as guides to its origin in some
35 Precambrian iron-formations: Fortschritte der Mineralogie, v. 56, p. 105–142.
- 36
- 37 Hofmann, H.J., 1976. Precambrian microflora, Belcher Islands, Canada; significance and
38 systematics. Journal of Paleontology 50, 1040-1073.
- 39 Hofmann, H.J., Grotzinger, J.P., 1985. Shelf-facies microbiotas from the Odjick and
40 Rocknest formations (Epworth Group; 1.89 Ga), northwestern Canada. Canadian
41 Journal of Earth Sciences 22, 1781-1792.
- 42 Holland, H.D. 2006. The oxygenation of the atmosphere and oceans. Philosophical
43 Transactions of the Royal Society, London, B-Biological Sciences 361, 903-915.
- 44 Hotinski, R.M., Kump, L.R., Arthur, M.A., 2004. The effectiveness of the
45 Paleoproterozoic biological pump: A $\delta^{13}\text{C}$ gradient from platform carbonates of

- the Pethei Group (Great Slave Lake Supergroup, NWT). Geological Society of America Bulletin 116, 539-554.
- House, C.H. et al., 2000. Carbon isotopic composition of individual Precambrian microfossils. *Geology* 28, 707-710.
- Johnston, D.T. et al., 2006. Evolution of the oceanic sulfur cycle at the end of the Paleoproterozoic. *Geochimica et Cosmochimica Acta*, 70(23): 5723-5739.
- Jones, J.A., Pirajno, F., Hocking, R.M., Grey, K., 2000. Revised stratigraphy for the Earahedy Group: implications for the tectonic evolution and mineral potential of the Earahedy Basin. *Geological Survey of Western Australia Annual Review*, 1999-2000, 57-64.
- Kaufman, A.J., Hayes, J.M., Klein, C., 1990. Primary and diagenetic controls of isotopic compositions of iron-formation carbonates. *Geochimica et Cosmochimica Acta* 54, 3461-3473.
- Kennedy, M.J., 1996. Stratigraphy, sedimentology, and isotopic geochemistry of Australian Neoproterozoic postglacial cap dolostones; deglaciation, $\delta^{13}\text{C}$ excursions, and carbonate precipitation. *Journal of Sedimentary Research* 66, 1050-1064.
- Klein, C. and Beukes, N.J., 1989. Geochemistry and sedimentology of a facies transition from limestone to iron-formation deposition in the early Proterozoic Transvaal Supergroup, South Africa. *Economic Geology*, 84(7): 1733-1774.
- Knauth, L.P. and Kennedy, M.J., 2009. The late Precambrian greening of the Earth. *Nature*, 460(7256): 728-732.
- Knoll, A.H., 2003. *Life on a Young Planet: The First Three Billion Years of Evolution on Earth*. Princeton University Press, Princeton NJ.
- Knoll, A.H. and Barghoorn, E.S., 1976. A Gunflint-type microbiota from the Duck Creek Dolomite, Western Australia. *Origins of Life and Evolution of Biospheres* 7, 417-423.
- Knoll, A.H., Simonson, B. 1981. Early Proterozoic microfossils and penecontemporaneous quartz cementation in the Sokoman Iron Formation, Canada. *Science* 211, 478-480.
- Knoll, A.H., Swett, K. 1990. Carbonate deposition during the late Proterozoic era: An example from Spitsbergen. *American Journal of Science* 290-A, 104-132.
- Knoll, A.H., Kaufman, A.J., Semikhatov, M.A., 1995. The carbon-isotopic composition of Proterozoic carbonates - Riphean successions from northwestern Siberia (Anabar Massif, Turukhansk Uplift). *American Journal of Science* 295, 823-850.
- Knoll, A.H., Strother, P.K., Rossi, S. 1988. Distribution and diagenesis of microfossils from the Lower Proterozoic Duck Creek Dolomite, Western Australia. *Precambrian Research* 38, 257-279.
- Lindsay, J.F., Brasier, M.D., 2002. Did global tectonics drive early biosphere evolution? Carbon isotope record from 2.6 to 1.9 Ga carbonates of Western Australian basins. *Precambrian Research* 114, 1-34.

- 1 Maliva, R., Knoll, A.H., Siever, R. 1989. Secular change in chert distribution: a
2 reflection of evolving biological participation in the silica cycle. *Palaios* 4, 519-
3 532.
- 4 Martin, D.M., Li, Z.X., Nemchin, A.A., Powell, C.M., 1998. A pre-2.2 Ga age for giant
5 hematite ores of the Hamersley province, Australia? *Economic Geology* 93, 1084-
6 1090.
- 7 Martin, D.M., Powell, C.M., George, A.D., 2000. Stratigraphic architecture and evolution
8 of the early Paleoproterozoic McGrath Trough, Western Australia. *Precambrian*
9 *Research* 99, 33-64.
- 10 Meunier, A., 2005. *Clays*. Springer, Berlin, 472 pp.
- 11 Nelson, D.R., 2003. Compilation of SHRIMP U-Pb zircon geochronology data, 2002.
12 Geological Survey of Western Australia Record, 2003(2).
- 13 Poulton, S.W., Fralick, P.W., Canfield, D.E., 2004. The transition to a sulphidic ocean
14 ~1.84 billion years ago. *Nature* 431, 173-177.
- 15 Robinson, J.L., Cavanaugh, C.M., 1995. Rubisco in chemoautotrophic symbioses:
16 Implications for the interpretation of stable carbon isotope values. *Limnology and*
17 *Oceanography* 40, 1496-1502.
- 18 Schidlowski, M., Hayes, J.M., Kaplan, I.R., 1983. Isotopic inferences of ancient
19 biochemistries: Carbon, sulfur, hydrogen, and nitrogen, *in* Schopf, J.W. (Ed.),
20 *Earth's Earliest Biosphere*. Princeton University Press, Princeton NJ.
- 21 Schopf, J.W. (Ed.), 1983. *Earth's Earliest Biosphere*. Princeton University Press,
22 Princeton NJ.
- 23 Scott, C., Lyons, T.W., Bekker, A., Shen, Y., Poulton, S.W. Chu, X., Anbar, A.D. 2008.
24 Tracing the stepwise oxygenation of the Proterozoic ocean. *Nature* 452, 456-458.
- 25 Shen, Y.N., Canfield, D.E., Knoll, A.H. 2002. Middle Proterozoic ocean chemistry:
26 Evidence from the McArthur Basin, northern Australia. *American Journal of*
27 *Science* 302, 81-109.
- 28 Shen, Y., Knoll, A.H., Walter, M.R. 2003. Evidence for low sulphate and anoxia in a
29 mid-Proterozoic marine basin. *Nature* 423, 632-635
- 30 Sircombe, K.N., 2003. Age of the Mt Boggola volcanic succession and further
31 geochronological constraint on the Ashburton Basin, Western Australia.
32 *Australian Journal of Earth Sciences* 50, 967-974.
- 33 Slack, J.F., Grenne, T., Bekker, A. 2009. Seafloor-hydrothermal Si-Fe-Mn exhalites in the
34 Pecos greenstone belt, New Mexico, and the redox state of ca. 1720 Ma deep
35 seawater. *Geosphere* 5(3), 302-314.
- 36
- 37 Smith, J.B. et al., 1998. The Sholl Shear Zone, west Pilbara: evidence for a domain
38 boundary structure from integrated tectonostratigraphic analyses, SHRIMP U-Pb dating
39 and isotopic and geochemical data of granitoids. *Precambrian Research*, 88(1-4): 143-
40 171.
- 41
- 42
- 43 Surge, D.M., Savarese, M., Dodd, J.R., Lohmann, K.C., 1997. Carbon isotopic evidence
44 for photosynthesis in Early Cambrian oceans. *Geology* 25, 503-506.

- 1 Thorne, A.M., 1983. Upward-shallowing sequences in the Precambrian duck Creek
2 Dolomite, Western Australia. Western Australia Geological Survey Professional
3 Papers 1985, 81-93.
- 4 Thorne, A.M., Seymour, D.B., 1991. Geology of the Ashburton Basin, Western Australia.
5 Bulletin (Geological Survey of Western Australia). Geological Survey of Western
6 Australia, Perth WA, 141 pp.
- 7 Tobin, K.J., 1990. The paleoecology and significance of the Gunflint-type microbial
8 assemblages from the Frere Formation (Early Proterozoic), Nabberu Basin,
9 Western Australia. *Precambrian Research* 47, 71-81.
- 10
- 11 Tosca, N.J., McLennan, S.M., Lindsley, D.H. and Schoonen, M.A.A., 2004. Acid-sulfate
12 weathering of synthetic Martian basalt: The acid fog model revisited. *J. Geophys. Res.*,
13 109.
- 14
- 15 Tyler, S.A., Barghoorn, E.S., 1954. Occurrence of structurally preserved plants in pre-
16 Cambrian rocks of the Canadian Shield. *Science* 119, 606-608.
- 17 Veizer, J., Clayton, R.N. and Hinton, R.W., 1992a. Geochemistry of Precambrian
18 carbonates: IV. Early Paleoproterozoic (2.25 ± 0.25 ga) seawater. *Geochimica et*
19 *Cosmochimica Acta* 56, 875-885.
- 20 Veizer, J., Plumb, K.A., Clayton, R.N., Hinton, R.W. and Grotzinger, J.P., 1992b.
21 Geochemistry of Precambrian carbonates: V. Late Paleoproterozoic seawater.
22 *Geochimica et Cosmochimica Acta* 56, 2487-2501.
- 23 Walter, M.R., Goode, A.D.T., Hall, J.A., 1976. Microfossils from the newly discovered
24 Precambrian stromatolitic iron formation in Western Australia. *Nature* 261,
25 221-223.
- 26
- 27 Walter, M.R., 1972. Stromatolites and the biostratigraphy of the Australian Precambrian
28 and Cambrian: *Special Papers in Paleontology* No. 11, 268 p.
- 29
- 30 Yui, S., 1966. Decomposition of siderite to magnetite at lower oxygen fugacities: a
31 thermochemical interpretation and geological implications. *Economic Geology*
32 61, 768-776.
- 33
- 34 Zempolich, W.G., Wilkinson, B.H., and Lohmann, K.C., 1988. Diagenesis of Late
35 Proterozoic carbonates: The Beck Spring Dolomite of eastern California. *Journal*
36 *of Sedimentary Petrology* 58, 656-672.
- 37
- 38

Figure Captions

Fig. 1. Tectonic map of Western Australia showing the location of the Capricorn Orogen and related sedimentary basins. Map of Wyloo Group exposed at Duck Creek Gorge, showing field relationship between units. Sections described in the text are marked.

Fig. 2. Stratigraphy and C and O isotope ratio data. Three negative $\delta^{13}\text{C}$ excursions are present. Oxygen isotope values ($\delta^{18}\text{O}$) follow deepening-upward sequences. Red values indicate samples from section F, capturing a local slumped and brecciated unit (see Plate 3). Sequence stratigraphic interpretations are shown: TST = Transgressive System Tract, MFI = Maximum Flooding Interval, HST = Highstand System Tract.

Fig. 3. (A) outcrop photo of Duck Creek Dolomite at Duck Creek Gorge, approximately 30 m of relief; (B) giant wave ripple, section G; (C) laminated precipitates truncated by planar-bedded carbonates suggestive of intertidal environments, section A; (D) mound-and-channel, section A; (E) iron formation, section A; (F) peritidal precipitates draping needle-like crystal fans, section B.

Fig. 4. (A) Low-relief domal precipitates, section B; (B) conical precipitates, section B; (C) early diagenetic chert nodule in iron formation, section C; (D) ironstone within section C; (E) and calcite-rich carbonate within iron formation, section C.

Fig. 5. (A) Slumped and brecciated unit with iron-stained matrix, section F; (B) early diagenetic and fossiliferous black chert, section C; (C) stylolitic limestones, section D; (D) dolomitic turbidite in stylolitic limestone, section E; (E) limestones, dolomitic turbidites, and siltstone unit at arrows, section E.

Fig. 6. Carbon isotope chemostratigraphy versus mineral abundances (determined by X-ray diffraction abundances). Shallow-water sections contain iron-rich carbonates, such as dolomite, ankerite, and Fe-dolomite (due to ferrous dolomitizing fluids). Deep-water sections are dominated by iron-poor carbonates, such as calcite and aragonite. Iron formations are rich in silica, iron, and clays. Potassium feldspars peak in abundance within the iron formation.

Fig. 7. X-ray diffraction trace, both glycolated and unglycolated, from a hematite-rich iron formation sample, showing the presence of berthierine, illite, and chlorite.

Fig. 8. (A) Crossplot of $\delta^{13}\text{C}$ and $\delta^{18}\text{O}$ values from the complete section. (B) Crossplot of $\delta^{13}\text{C}$ and $\delta^{18}\text{O}$ values from samples between 600 and 700 meters. Samples which are depleted in ^{13}C are enriched in ^{18}O .

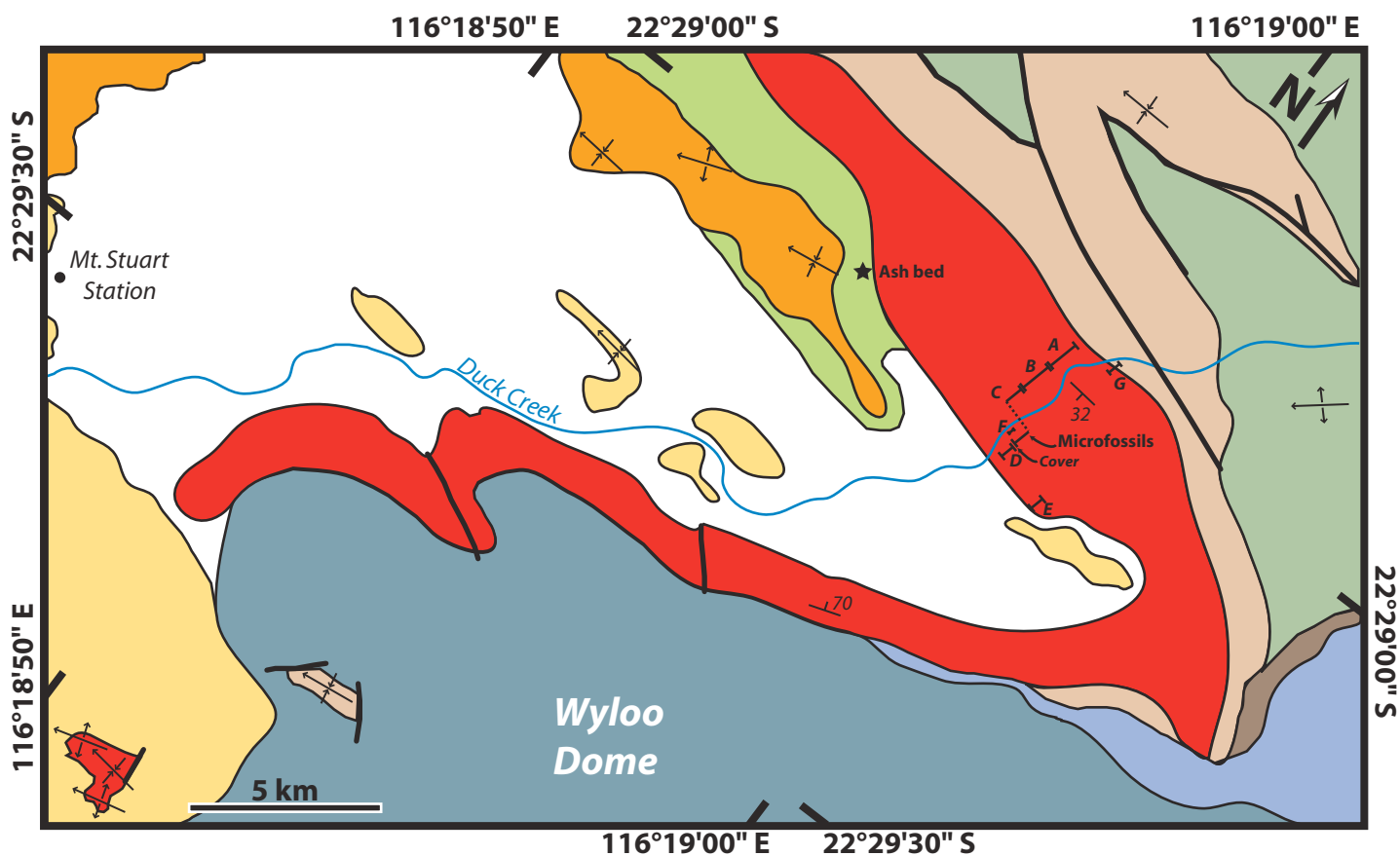
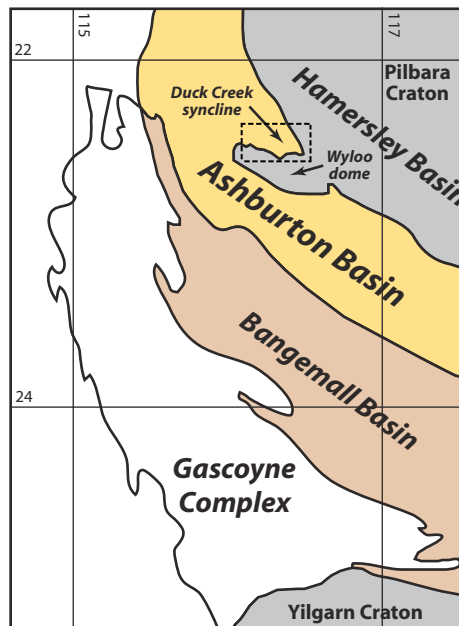
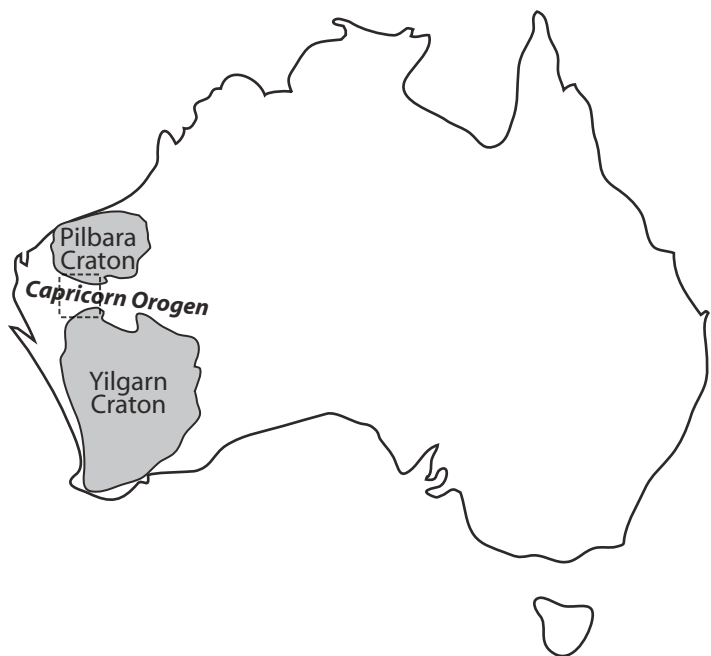
Fig. 9: (A) Chert 25 at 40x, showing *Eoastrion*, *Gunflintia*, and *Huroniospora*; (B) petrographic thin section of sample F0 at 40x showing iron staining on carbonate grains.

Fig. 10: Marine cross-section showing a summary of mid-Paleoproterozoic microfossil distributions. Previous Gunflint-type microbiotas occur in cherty stromatolites deposited in relatively shallow water (Amard and Bertrand-Safarti, 1997; Barghoorn and Tyler, 1965; Knoll and Simonson, 1981; Walter et al., 1976; Tobin, 1990), whereas fossiliferous cherts from the Belcher Islands contain coccoidal cyanobacteria from the shallowest water depths (Hofmann, 1976; Golubic and Hofmann, 1976). The occurrence of a Gunflint-type assemblage in early diagenetic Duck Creek Formation cherts is useful because its stratigraphic context places Gunflint-type microfossils in an iron-rich deep water paleoenvironment. This relationship lends support to the proposed identification of these organisms as bacteria with iron-based metabolisms, as suggested by Cloud (1965).

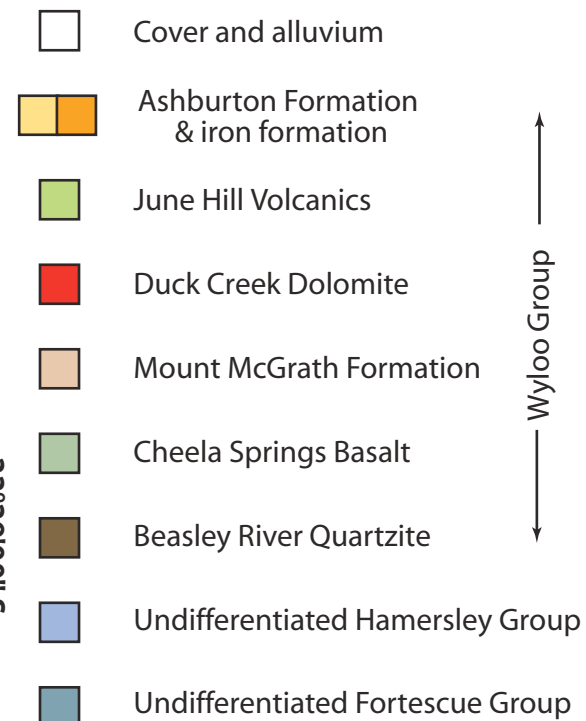
Appendix 1: Oxygen and carbon isotope composition of samples.

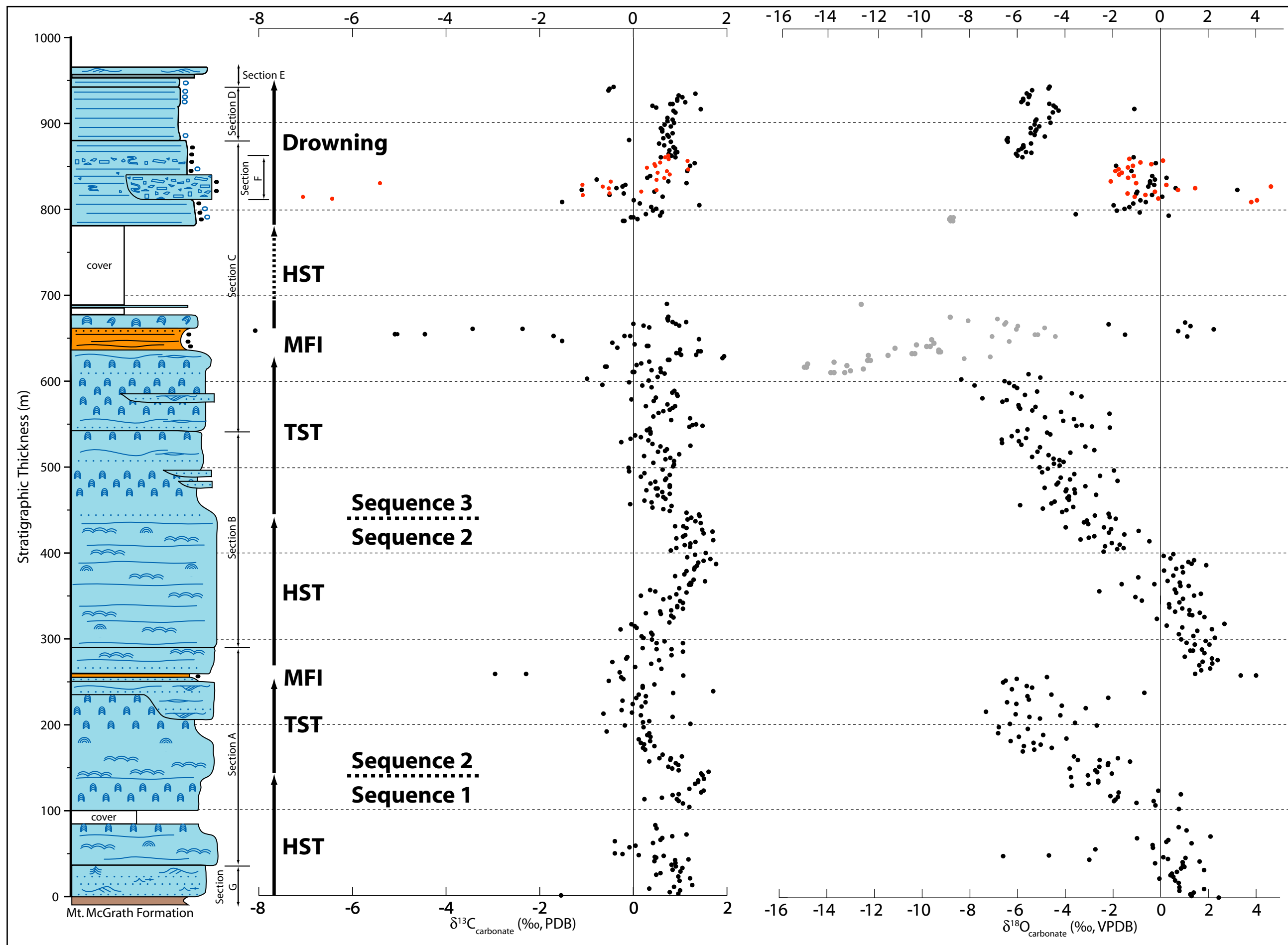
Appendix 2: Stratigraphic distribution of minerals, based on X-ray diffraction analysis.

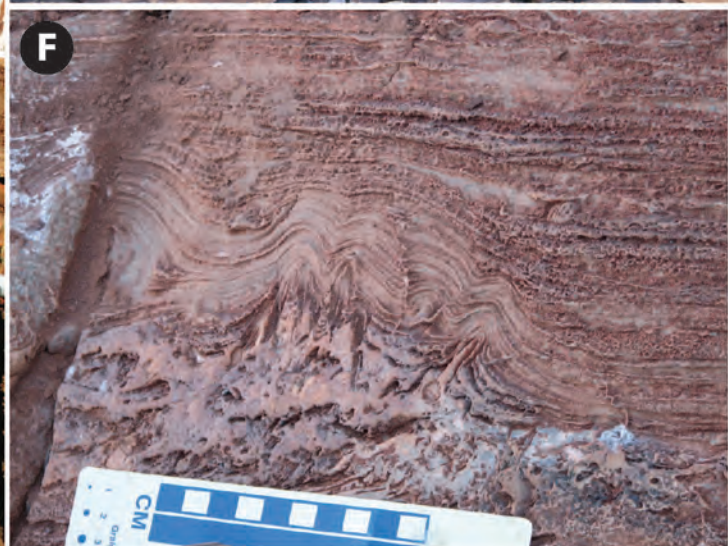
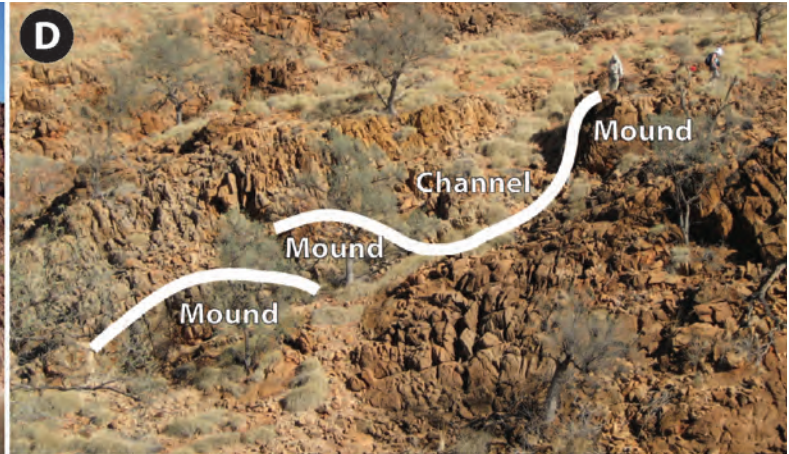
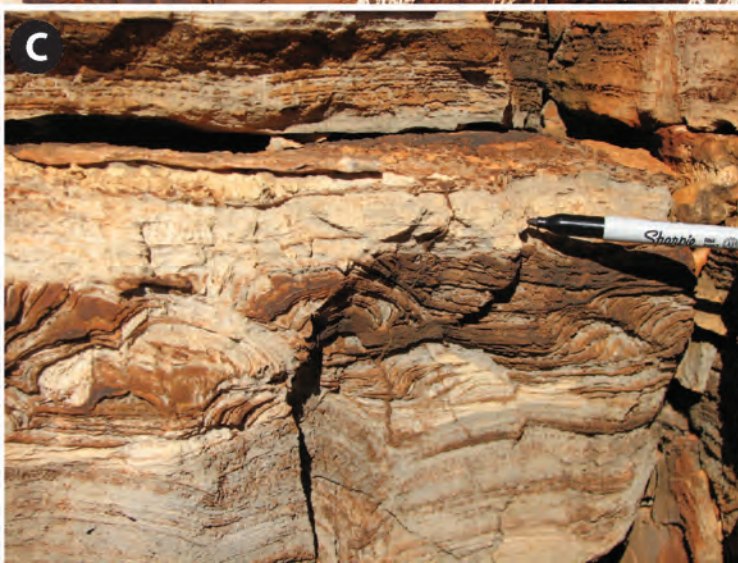
Appendix 3: U-Pb SHRIMP zircon data.

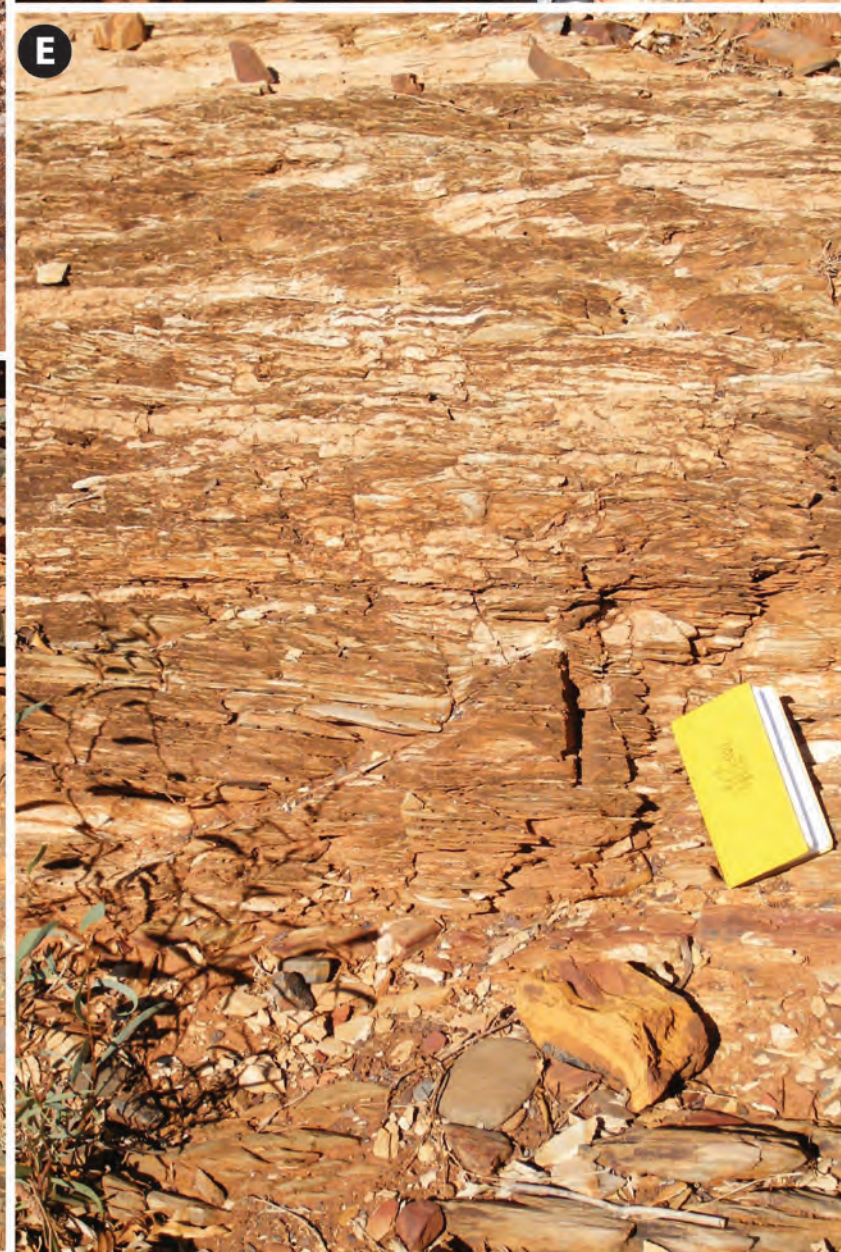
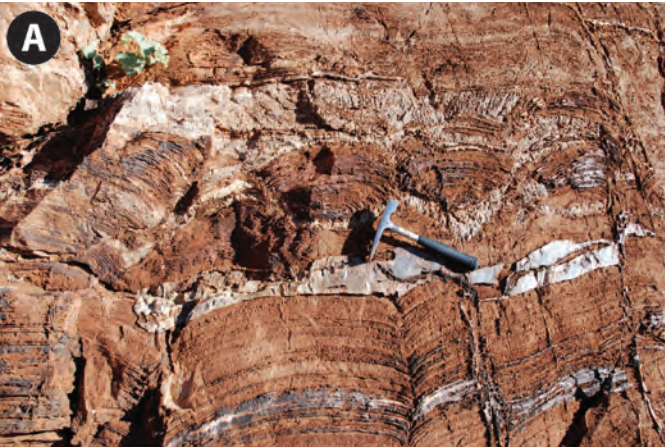


Duck Creek syncline stratigraphy

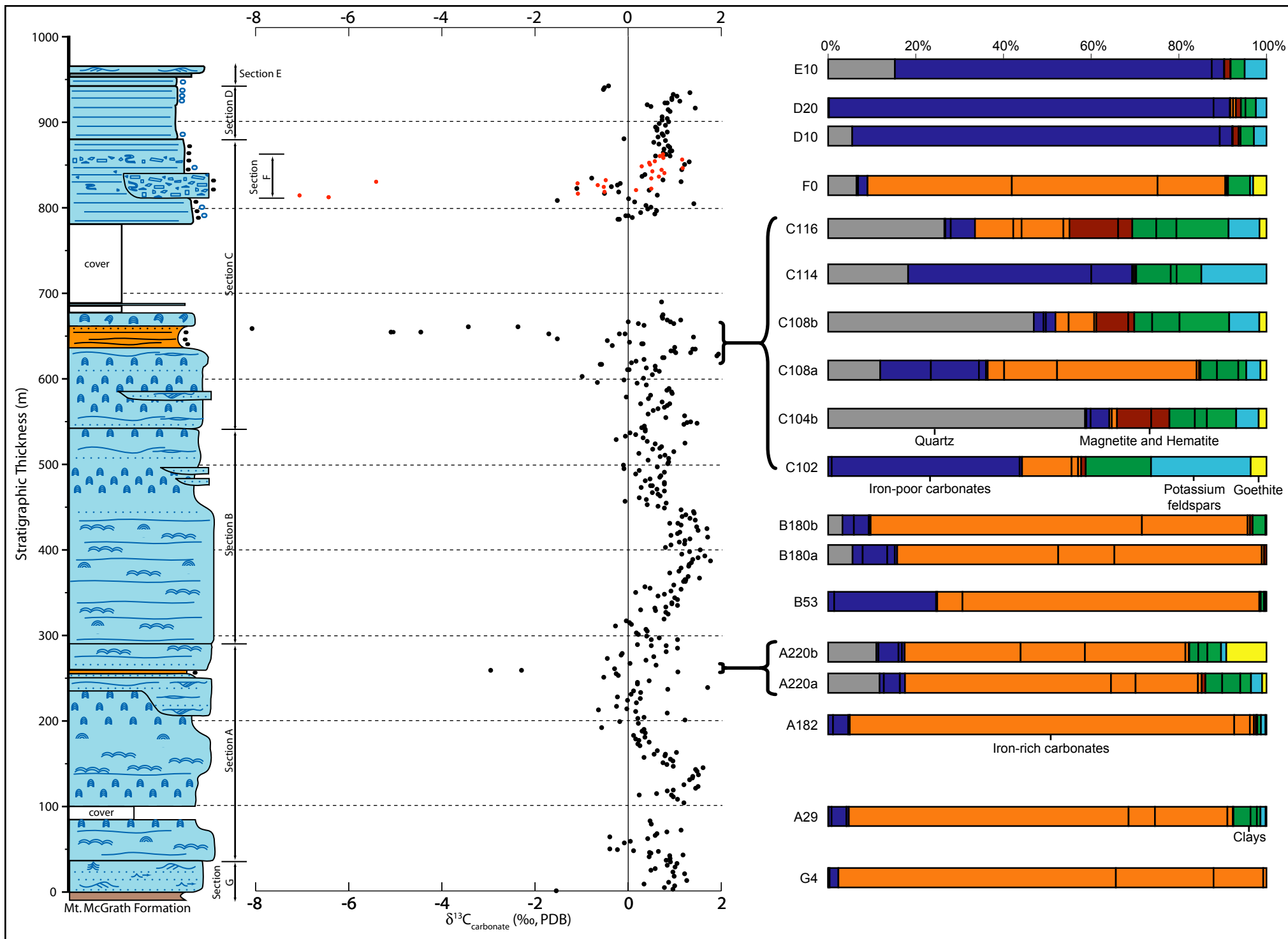


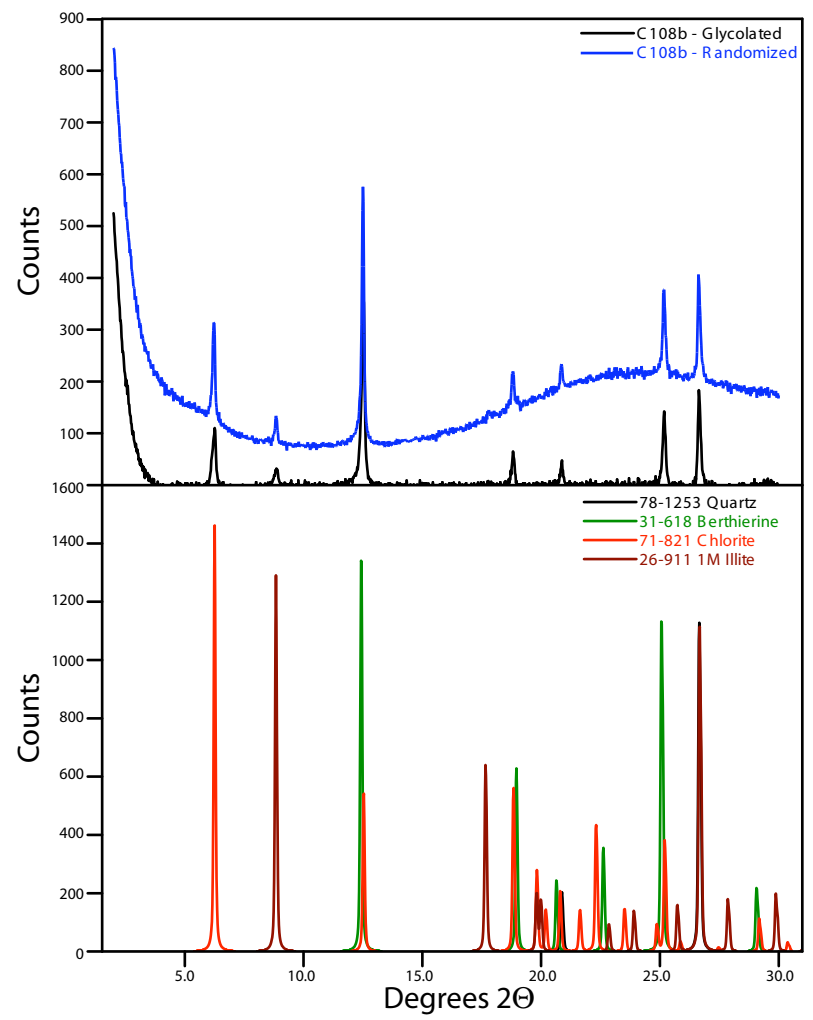


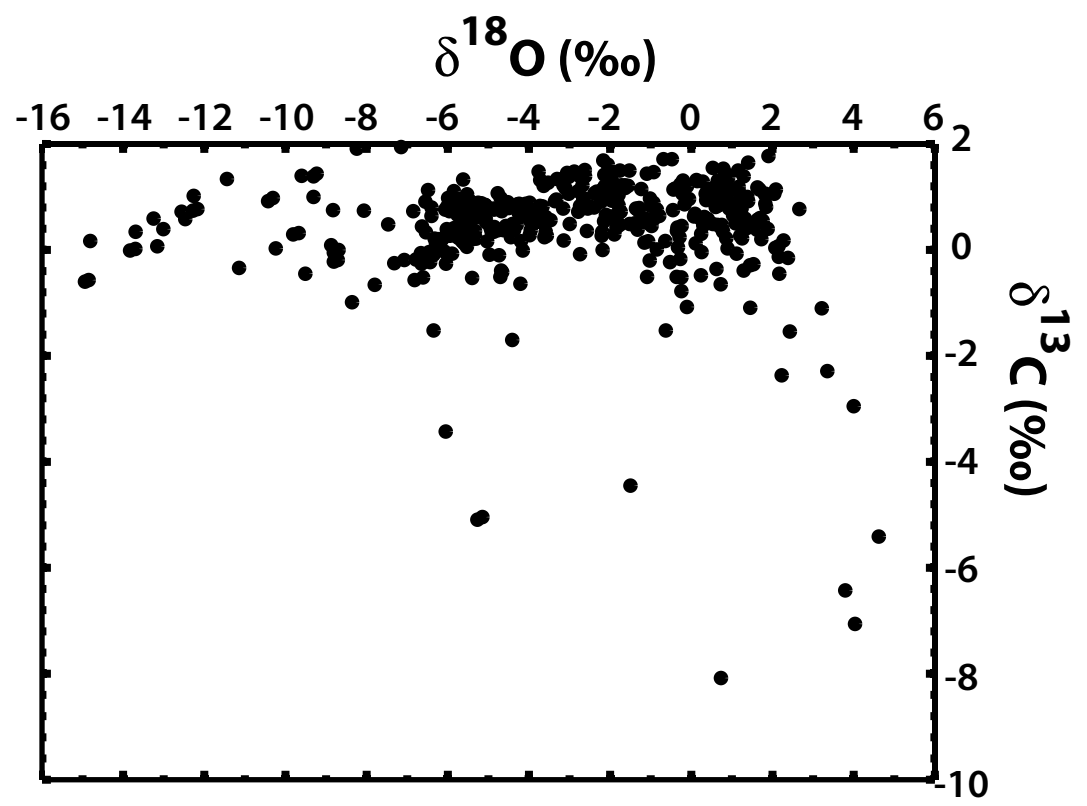


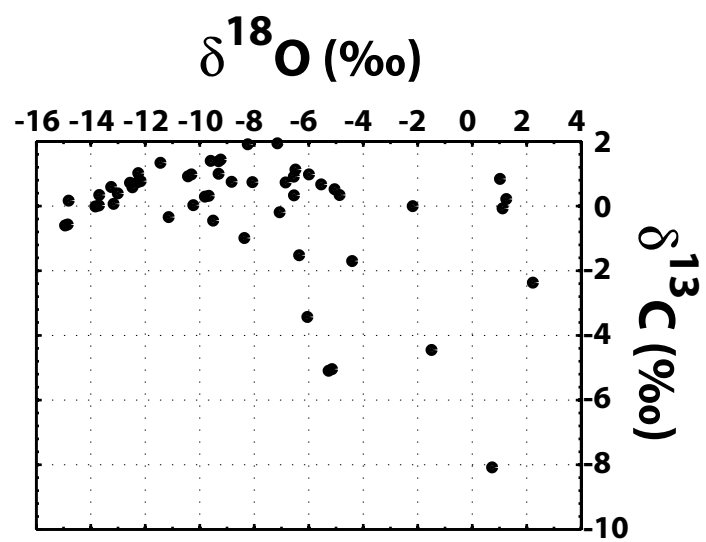


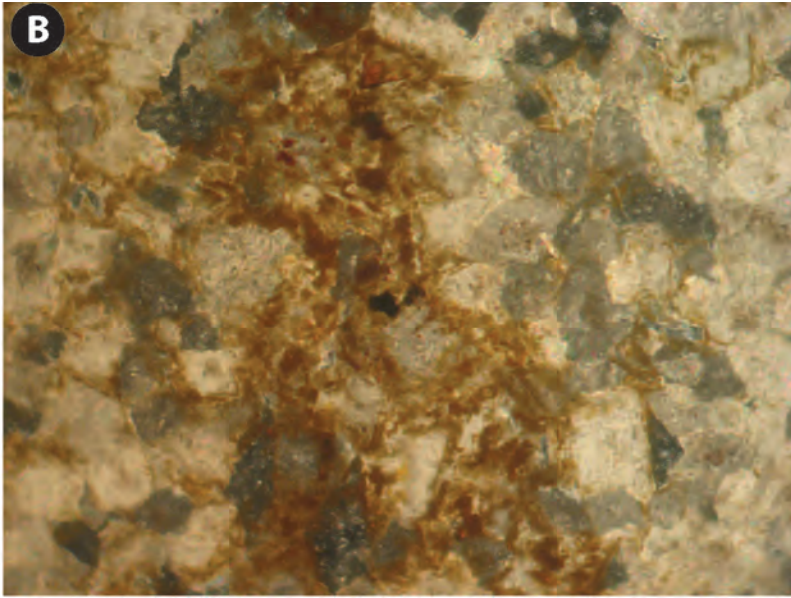
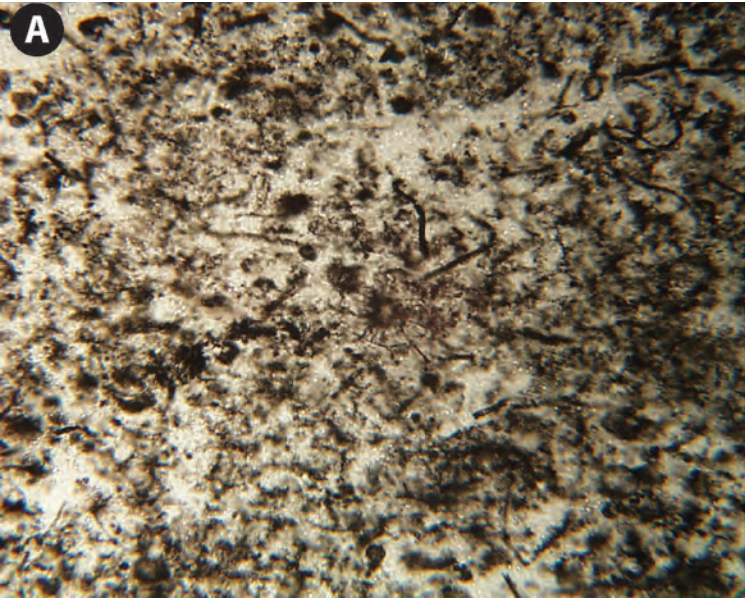


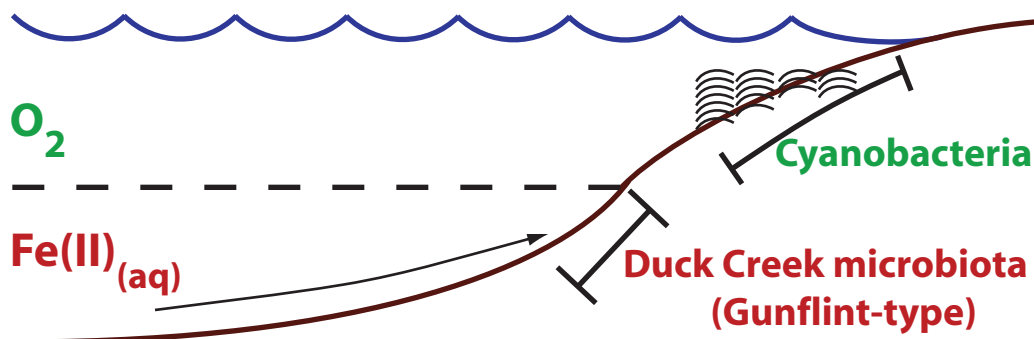


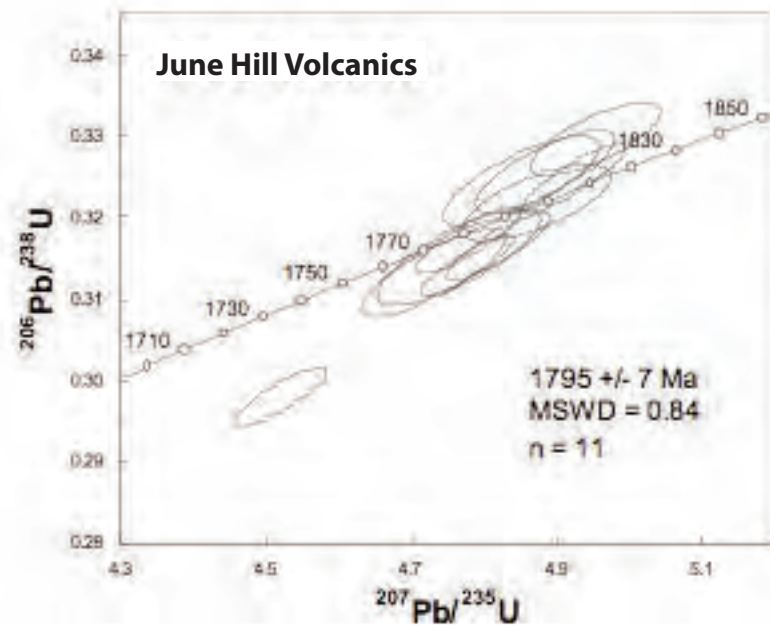












Section	Sample ID	Sample meterage	$\delta^{18}\text{O}$ final	$\delta^{13}\text{C}$ final
G	000	000	2.428	-1.54
G	002	002	1.289	0.96
G	004	004	1.238	0.78
G	006	006	1.382	1.00
G	008	008	0.786	0.34
G	010	010	1.821	0.87
G	012	012	0.778	1.26
G	017	017	0.753	0.99
G	020	020	0.604	1.21
G	022	022	-0.059	0.96
G	024	024	0.529	0.49
G	026	026	0.409	0.58
G	028	028	0.465	1.01
G	030	030	0.675	0.84
G	032	032	1.813	1.05
G	034	034	0.849	0.91
G	036	036	0.99	0.82
G	038	038	0.939	0.90
A	002	040	-0.238	0.45
A	003	041	0.924	0.89
A	004	042	1.629	1.18
A	006	044	-2.995	0.49
A	007	045	0.299	0.46
A	008	046	1.029	0.65
A	009	047	0.105	0.12
A	010	048	-6.608	-0.23
A	011	049	-4.688	-0.39
A	018	056	-2.743	-0.08
A	020	058	-0.331	0.05
A	023	061	-0.344	0.42
A	025	063	1.286	-0.39
A	027	065	0.237	0.58
A	029	067	0.32	0.62
A	031	069	-0.991	0.83
A	033	071	2.084	1.14
A	040	078	1.089	0.50
A	044	082	0.75	0.47
A	065	103	0.76	1.20
A	069	107	-0.219	1.06
A	072	110	-1.017	0.97
A	074	112	-0.288	0.24
A	074	112	-1.965	0.93
A	076	114	-1.898	0.61
A	079	117	-1.793	0.84
A	080	118	-2.108	0.97
A	082	120	0.837	1.45
A	084	122	-1.762	1.50
A	086	124	-0.108	1.20
A	092	130	-3.726	1.32
A	094	132	-3.021	1.38
A	096	134	-2.617	1.39

A	098	136	-2.623	1.51
A	102	140	-3.761	1.48
A	104	142	-3.061	1.45
A	106	144	-2.056	1.61
A	108	146	-2.663	0.97
A	110	148	-2.743	0.83
A	112	150	-3.817	0.75
A	114	152	-2.582	0.96
A	116	154	-2.22	0.91
A	118	156	-2.195	0.34
A	120	158	-1.285	0.79
A	122	160	-3.468	0.56
A	122	160	-2.566	0.80
A	124	162	-1.793	1.04
A	126	164	-3.637	0.63
A	132	170	-5.776	0.25
A	134	172	-5.307	0.21
A	136	174	-4.569	0.45
A	138	176	-5.742	0.23
A	140	178	-5.029	0.16
A	142	180	-5.331	0.36
A	144	182	-6.291	0.12
A	147	185	-3.955	0.37
A	149	187	-5.948	0.30
A	151	189	-4.922	0.34
A	153	191	-6.82	-0.57
A	158	196	-5.579	0.22
A	160	198	-6.785	-0.18
A	162	200	-2.68	1.22
A	164	202	-6.321	0.21
A	165	203	-3.588	0.34
A	170	208	-5.07	0.84
A	172	210	-5.507	0.16
A	174	212	-4.211	-0.64
A	175	213	-6.082	-0.03
A	178	216	-7.319	-0.25
A	182	220	-3.142	0.18
A	185	223	-4.153	-0.01
A	187	225	-6.057	0.26
A	189	227	-6.436	-0.23
A	192	230	-5.53	0.06
A	194	232	-2.206	0.27
A	196	234	-5.595	0.12
A	198	236	-4.59	0.85
A	200	238	-0.685	1.71
A	204	242	-6.24	0.20
A	206	244	-5.397	0.20
A	208	246	-5.622	0.45
A	212	250	-6.611	-0.52
A	214	252	-6.505	-0.21
A	216	254	-6.042	-0.26
A	218	256	-4.772	1.07

A	220	258	4	-2.95
A	220	258	3.352	-2.29
A	222	260	1.446	-0.29
A	226	264	1.69	0.60
A	228	266	2.069	0.04
A	232	270	1.615	0.38
A	234	272	2.167	-0.45
A	236	274	1.758	0.55
A	238	276	2.383	-0.15
A	240	278	2.153	-0.13
A	242	280	1.009	0.82
A	246	284	1.83	1.06
A	249	287	1.238	0.82
A	249	287	1.354	0.50
A	250	288	1.726	0.20
B	000	294	1.42	0.50
A	256	294	2.044	1.06
B	002	296	1.09	0.67
B	004	298	1.884	0.40
B	006	300	0.862	0.22
B	008	302	2.27	0.18
B	010	304	1.371	0.41
B	012	306	0.762	0.38
B	016	310	1.531	-0.27
B	018	312	2.148	0.07
B	020	314	0.897	0.03
B	022	316	0.253	-0.04
B	024	318	2.664	0.77
B	030	324	-0.165	0.86
B	032	326	1.839	0.81
B	034	328	1.322	0.59
B	035	329	1.205	0.27
B	037	331	1.635	0.57
B	038	332	0.598	0.81
B	040	334	1.197	1.06
B	042	336	0.897	0.94
B	043	337	0.366	0.94
B	047	341	0.351	1.06
B	049	343	0.784	1.00
B	051	345	-0.793	0.64
B	053	347	0.932	0.78
B	055	349	-1.061	0.16
B	057	351	1.398	0.92
B	059	353	1.682	1.14
B	060	354	0.643	0.47
B	062	356	-2.571	0.36
B	064	358	0.589	0.98
B	068	362	1.17	1.19
B	068	362	0.832	1.23
B	070	364	-1.639	1.22
B	070	364	-0.27	1.24
B	072	366	0.79	1.53

B	074	368	0.283	1.29
B	078	372	-0.934	0.89
B	080	374	0.526	1.09
B	084	378	0.94	1.14
B	086	380	0.144	1.30
B	088	382	0.653	1.31
B	090	384	0.907	1.36
B	092	386	1.899	1.77
B	094	388	1.291	1.39
B	096	390	1.156	1.50
B	098	392	1.4	1.65
B	100	394	0.411	1.15
B	103	397	0.126	1.32
B	105	399	0.53	1.55
B	108	402	-2.396	0.80
B	111	405	-1.831	0.92
B	112	406	-1.561	1.21
B	114	408	-2.335	1.10
B	116	410	-1.723	1.22
B	118	412	-2.047	1.33
B	120	414	-0.48	1.71
B	122	416	-3.363	0.92
B	124	418	-3.019	1.06
B	126	420	-2.788	1.11
B	128	422	-1.525	1.50
B	130	424	-2.17	1.69
B	132	426	-0.927	1.47
B	134	428	-2.084	1.14
B	136	430	-3.984	0.89
B	136	430	-2.383	1.07
B	140	434	-3.039	1.44
B	142	436	-3.215	1.33
B	144	438	-3.098	1.16
B	146	440	-1.89	1.24
B	148	442	-2.144	1.42
B	150	444	-2.762	1.40
B	152	446	-2.19	1.14
B	154	448	-4.139	0.78
B	156	450	-3.953	0.64
B	158	452	-4.944	0.41
B	160	454	-3.662	0.82
B	162	456	-5.895	-0.07
B	164	458	-4.581	0.39
B	166	460	-4.444	0.24
B	168	462	-3.844	0.69
B	170	464	-3.912	0.64
B	172	466	-3.846	0.52
B	174	468	-2.705	0.78
B	176	470	-3.591	0.62
B	178	472	-3.981	0.28
B	180	474	-3.614	0.48
B	180	474	-3.948	0.52

B	182	476	-4.87	0.78
B	184	478	-3.158	0.78
B	186	480	-4.366	0.37
B	188	482	-4.304	0.47
B	190	484	-1.807	0.68
B	192	486	-3.803	0.70
B	194	488	-4.199	0.16
B	196	490	-2.551	0.78
B	198	492	-3.619	0.24
B	200	494	-4.975	-0.09
B	202	496	-1.955	0.63
B	204	498	-4.736	-0.10
B	206	500	-5.085	0.85
B	208	502	-4.242	0.87
B	210	504	-4.478	0.43
B	212	506	-4.079	0.87
B	214	508	-4.248	0.69
B	216	510	-4.497	0.79
B	218	512	-5.393	0.23
B	220	514	-4.699	0.98
B	223	517	-3.786	0.53
B	224	518	-5.164	0.68
B	226	520	-2.786	0.72
B	229	523	-5.061	0.58
B	230	524	-3.154	1.22
B	232	526	-5.845	0.41
B	234	528	-6.648	-0.26
B	236	530	-5.94	0.32
B	238	532	-6.66	-0.06
B	240	534	-5.651	0.16
B	242	536	-6.248	0.04
B	244	538	-4.628	0.37
B	246	540	-4.76	0.37
B	248	542	-6	0.29
B	250	544	-5.592	0.35
C	002	546	-2.134	1.20
C	003	547	-2.883	1.48
C	004	548	-3.528	1.27
C	005	549	-3.31	1.34
C	010	554	-4.082	0.81
C	012	556	-3.642	1.21
C	014	558	-4.853	0.43
C	018	562	-2.149	0.54
C	020	564	-4.181	0.64
C	022	566	-5.384	0.78
C	024	568	-5.896	0.84
C	026	570	-5.252	0.89
C	026	570	-5.948	0.27
C	028	572	-5.962	0.73
C	032	576	-6.637	0.44
C	034	578	-6.46	-0.04
C	036	580	-7.472	0.48

C	038	582	-3.326	0.95
C	040	584	-5.7	0.93
C	042	586	-3.733	0.83
C	044	588	-5.175	0.88
C	048	592	-6.023	0.39
C	050	594	-6.146	0.19
C	051	595	-7.798	-0.66
C	054	598	-6.353	-0.09
C	056	600	-6.54	0.33
C	058	602	-8.362	-0.99
C	060	604	-5.055	0.52
C	064	608	-5.544	0.67
C	066	610	-13.25	0.59
C	066	610	-13.70	0.02
C	066	610	-13.83	-0.01
C	068	612	-13.01	0.39
C	070	614	-12.47	0.58
C	072	616	-14.85	-0.57
C	072	616	-14.94	-0.60
C	074	618	-13.16	0.07
C	076	620	-14.81	0.17
C	078	622	-13.69	0.34
C	080	624	-12.17	0.77
C	080	624	-12.28	0.74
C	082	626	-8.24	1.91
C	084	628	-7.15	1.94
C	086	630	-12.26	1.02
C	086	630	-11.44	1.34
C	088	632	-10.31	0.98
C	088	632	-10.43	0.92
C	090	634	-9.23	1.44
C	090	634	-9.31	1.39
C	092	636	-9.31	1.00
C	094	638	-11.14	-0.34
C	096	640	-9.67	0.32
C	096	640	-9.81	0.29
C	098	642	-10.24	0.03
C	100	644	-9.51	-0.45
C	102	646	-6.35	-1.52
C	104	648	-9.60	1.40
C	108	652	1.114	-0.07
C	108	652	-7.07	-0.19
C	108	652	-4.41	-1.70
C	110	654	-1.496	-4.45
C	110	654	-5.15	-5.04
C	110	654	-5.27	-5.09
C	114	658	0.732	-8.08
C	116	660	2.223	-2.37
C	116	660	-6.05	-3.43
C	118	662	-4.87	0.34
C	120	664	1.249	0.22
C	120	664	-5.99	0.98

C	122	666	-2.186	0.00
C	122	666	-6.55	0.91
C	124	668	1.019	0.84
C	124	668	-6.49	1.13
C	126	670	-8.07	0.74
C	128	672	-6.85	0.73
C	130	674	-8.83	0.75
C	145	689	-12.56	0.72
C	242	786	-8.71	-0.19
C	242	786	-8.81	-0.22
C	244	788	-8.87	0.09
C	246	790	-8.69	0.00
C	246	790	-8.81	-0.05
C	248	792	0.339	0.57
C	250	794	-3.559	0.27
C	252	796	-0.886	0.61
C	254	798	-1.848	0.42
C	256	800	-1.52	0.49
C	258	802	-1.323	0.38
C	260	804	-1.969	1.41
C	262	806	-1.156	0.14
F	000	808	3.79	-6.43
C	264	808	-0.625	-1.52
F	002	810	4.037	-7.06
C	266	810	-0.851	0.01
F	004	812	-0.109	-1.08
F	006	814	-1.092	-0.51
C	270	814	0.065	0.63
F	008	816	-0.644	0.17
C	272	816	-0.362	-0.51
F	010	818	-1.395	0.50
C	274	818	-1.024	-0.20
F	012	820	-0.241	-0.52
C	276	820	-0.982	0.45
F	014	822	0.725	-0.65
C	278	822	3.216	-1.10
F	016	824	1.449	-1.09
C	280	824	0.624	-0.36
F	018	826	4.622	-5.41
C	282	826	-0.525	-0.23
F	020	828	0.237	-0.48
C	284	828	-0.273	-0.17
F	022	830	-1.036	0.50
C	286	830	-0.443	1.14
F	024	832	-2.101	0.66
C	288	832	-0.452	0.75
C	290	834	-0.244	-0.78
F	028	836	-1.366	0.78
C	292	836	0.247	0.30
F	030	838	-1.126	0.52
C	294	838	-0.357	0.36
F	032	840	-1.741	0.72

F	034	842	-1.627	1.17
F	036	844	-1.9	0.29
C	300	844	-1.233	1.15
F	038	846	-1.767	0.47
F	040	848	-1.374	0.45
F	042	850	-1.161	0.57
C	306	850	-1.869	1.21
F	044	852	-0.396	1.16
C	309	853	-0.205	1.31
F	046	854	-0.85	0.76
F	048	856	0.091	0.68
F	050	858	-1.31	0.75
D	000	860	-5.789	0.90
C	316	860	-1.139	0.59
D	002	862	-6.01	0.82
D	004	864	-6.067	0.76
D	005	865	-5.415	0.90
D	006	866	-5.653	0.94
D	008	868	-5.97	0.77
D	010	870	-5.826	0.89
D	012	872	-5.757	0.86
D	014	874	-5.762	0.66
D	016	876	-5.437	0.55
D	018	878	-6.404	0.80
D	020	880	-6.455	-0.09
D	022	882	-6.403	0.64
D	024	884	-4.858	0.76
D	026	886	-5.284	0.73
D	028	888	-5.459	0.84
D	030	890	-5.263	0.62
D	032	892	-5.213	0.62
D	034	894	-5.455	0.59
D	036	896	-5.094	0.80
D	038	898	-5.285	0.67
D	040	900	-4.623	0.87
D	042	902	-5.263	0.73
D	044	904	-5.218	0.84
D	046	906	-4.672	0.73
D	052	912	-4.524	0.90
D	054	914	-4.283	0.86
D	056	916	-1.1	1.44
D	058	918	-4.405	0.49
D	060	920	-4.494	0.41
E	000	922	-5.572	0.84
D	062	922	-4.672	0.79
E	002	924	-5.847	1.11
E	004	926	-5.765	0.94
E	006	928	-5.764	0.94
E	008	930	-5.528	1.05
E	010	932	-5.502	0.97
E	012	934	-5.621	1.33
E	016	938	-5.398	-0.53

E	018	940	-4.704	-0.51
E	020	942	-4.662	-0.42

Sample Name	#	Quartz	Calcite	Mg-calcite	Aragonite	Dolomite	Fe-Dolomite	Ankerite	Magnesite	Siderite	Halite	Pyrite	Anhydrite	Magnetite	Hematite	Goethite
E10	18	15.2	71.9	2.8	0.0	0.0	0.0	0.0	0.0	0.0	0.2	0.0	0.1	0.0	1.4	0.0
D20	17	0.2	85.6	3.6	0.0	0.6	0.0	0.6	0.1	0.0	0.2	0.0	0.0	0.0	1.1	0.0
D10	16	5.4	82.7	2.8	0.0	0.0	0.0	0.1	0.0	0.0	0.2	0.0	0.1	0.0	1.3	0.0
F0	15	6.4	0.4	2.1	0.0	32.5	32.8	15.3	0.0	0.3	0.3	0.1	0.0	0.0	0.3	3.0
C116	14	25.3	0.2	1.2	0.0	8.3	1.8	9.1	5.3	1.3	0.2	0.0	0.2	3.1	10.6	1.5
C114	13	17.8	40.8	9.1	0.0	0.2	0.0	0.4	0.1	0.0	0.1	0.1	0.1	0.1	0.1	0.0
C108b	12	45.5	2.2	0.5	0.0	2.9	0.0	5.7	2.1	0.5	0.2	0.0	0.1	1.3	7.1	1.6
C108a	11	11.7	11.4	10.8	1.6	3.7	11.9	31.5	0.4	0.6	0.2	0.2	0.0	0.0	0.3	1.4
C104b	10	53.6	0.3	0.0	0.9	0.5	0.0	0.0	3.9	1.1	0.1	0.0	0.4	3.8	7.2	1.6
C102	9	0.0	0.8	42.0	0.0	11.1	0.0	1.4	0.6	0.7	0.6	0.1	1.4	1.0	0.0	3.5
B180b	8	3.2	2.6	3.3	0.2	60.7	0.0	23.6	0.2	0.5	0.4	0.1	0.0	0.0	0.6	0.0
B180a	7	5.5	2.3	5.6	1.7	36.7	12.8	33.6	0.6	0.5	0.0	0.2	0.0	0.0	0.5	0.0
B53	6	0.0	1.4	23.0	0.0	0.0	5.7	67.0	0.3	0.1	0.2	0.0	0.0	0.0	0.2	0.3
A220b	5	10.8	0.5	4.5	0.8	25.9	14.4	22.5	0.6	0.8	0.6	0.3	0.0	0.0	0.1	9.0
A220a	4	11.3	0.9	3.5	0.0	45.2	5.4	13.7	1.1	0.8	0.5	0.2	0.0	0.0	0.8	1.0
A182	3	0.0	1.1	3.4	0.3	86.5	0.0	3.5	0.1	0.9	0.9	0.0	0.0	0.0	0.5	0.2
A29	2	0.1	0.7	3.3	0.0	62.3	5.9	16.1	0.5	1.2	1.2	0.2	0.0	0.0	0.2	0.2
G4	1	0.0	0.3	2.0	0.0	62.7	22.1	11.2	0.0	0.7	0.9	0.0	0.0	0.0	0.0	0.0

Anatase	Rutile	ordered Microcline feldspar	intermediate Microcline feldspar	Sanidine feldspar	Orthoclase feldspar	Oligoclase feldspar (North Carolina)	Total non- clays	Na-Smectite (Wyo)	Ca-smectite (Wyo)	1Md illite (+ dioct mica & smectite)
0.0	0.2	0.0	0.1	0.5	0.0	4.3	96.8			
0.0	0.2	0.4	0.3	0.0	0.3	1.4	94.6			
0.1	0.2	0.1	0.1	0.5	0.5	1.6	95.8			1.0
0.0	0.0	0.0	0.0	0.0	0.0	0.7	94.0			1.6
0.0	0.0	0.8	1.8	2.5	0.4	1.2	74.8			0.0
0.0	0.0	0.0	2.0	7.6	4.7	0.3	83.4			0.3
0.0	0.0	0.2	3.0	2.7	0.5	0.2	76.2			1.7
0.0	0.0	0.0	0.8	1.2	0.8	0.5	89.0			0.8
0.0	0.0	0.0	2.3	0.5	0.4	1.6	78.1			
0.0	0.0	0.0	7.8	3.5	8.5	2.4	85.4			
0.0	0.0	0.0	0.0	0.0	0.0	0.2	95.6			1.1
0.0	0.0	0.0	0.0	0.0	0.0	0.0	100.0			
0.0	0.0	0.0	0.0	0.1	0.2	0.0	98.6			0.7
0.0	0.0	0.1	0.1	0.0	0.5	0.5	91.8			2.8
0.0	0.0	0.3	1.2	0.0	0.0	0.9	86.8			2.4
0.0	0.0	0.0	0.0	0.4	0.0	0.6	98.5			
0.0	0.0	0.0	0.0	0.7	0.0	0.5	93.0			0.8
0.0	0.0	0.0	0.0	0.0	0.0	0.0	100.0			

1M Illite (R>2; 88%I)	1M illite (R>1, 70- 80%I)	Glauconite	Biotite (2M1)	Berthierine	Muscovite (2M1)	Illite (1M, PD3B)	Montmorillonite (Webster Pass)	Chlorite	Fe-chlorite	Total clays	Total detrital component	Other clays	Stratigraphic height in meters
1.4		1.0						1.8		3.2	4.9	3.2	932
		0.4		0.0			0.7	2.3		3.3	2.4	2.3	880
	0.0				3.1			1.3		3.5	2.8	3.0	870
6.3		5.2		4.4		0.6	0.4	0.2		4.9	0.7	4.9	808
		7.7		1.3	3.7		1.5	4.0		20.9	6.7	11.3	660
		4.0		6.1						14.5	14.5	5.5	658
		3.7		4.8				6.3	2.9	21.0	6.7	11.0	652
1.4		5.3		2.5			1.2	1.0		10.3	3.2	1.8	652
				14.6				3.5		13.9	4.7	6.1	648
				0.0						14.6	22.3	0.0	646
								1.7		2.9	0.2	2.9	474
										0.0	0.0	0.0	474
										0.7	0.3	0.7	347
		2.0		2.0				0.3		7.1	1.2	3.1	258
		3.7		4.0						10.0	2.4	2.4	258
0.6		0.1		0.2				0.2		1.1	1.0	0.8	220
		3.8		1.4						6.0	1.2	0.8	67
										0.0	0.0	0.0	4

Table 3: SHRIMP isotopic data for zircons from the June Hill Tuff (Mount 09-20B).

Grain-spot	U (ppm)	Th (ppm)	²³² Th / ²³⁸ U	% common 206Pb	²⁰⁷ Pb / ²⁰⁶ Pb	+/-1σ	²⁰⁷ Pb / ²³⁵ U	+/-1σ	²⁰⁶ Pb / ²³⁸ U	+/-1σ	²⁰⁷ Pb / ²⁰⁶ Pb Age (Ma)	+/-1σ	Conc. (%)
Magmatic population													
1-Aug	362	87	0.25	0	0.1104	0.0005	4.82	0.05	0.317	0.003	1806	9	102
2-Aug	564	208	0.38	0.07	0.1102	0.0005	4.77	0.04	0.314	0.002	1803	7	102
1-Nov	673	442	0.68	0.22	0.1099	0.0005	4.52	0.04	0.298	0.002	1799	9	107
28-1	405	77	0.2	0.01	0.1098	0.0005	4.92	0.05	0.325	0.003	1797	8	99
23-1	231	52	0.23	0.02	0.1097	0.0011	4.87	0.07	0.322	0.003	1795	18	100
18-1	119	43	0.37	0.18	0.1096	0.001	4.76	0.07	0.315	0.004	1793	17	101
30-1	151	45	0.3	0.04	0.1095	0.0009	4.73	0.07	0.313	0.004	1790	15	102
1-Oct	422	125	0.3	0.08	0.1092	0.0006	4.78	0.05	0.317	0.003	1785	10	100
17-1	322	56	0.18	0.34	0.1089	0.0009	4.95	0.06	0.33	0.003	1781	14	97
20-1	198	182	0.95	0.12	0.1087	0.0009	4.88	0.06	0.326	0.003	1777	15	98
1-Sep	146	39	0.28	0.11	0.1083	0.001	4.85	0.07	0.325	0.004	1772	17	98
Older zircons													
1-Jul	272	333	1.27	0	0.3	0.0008	29.25	0.28	0.707	0.006	3470	4	101
27-1	82	93	1.17	0.17	0.1817	0.0015	12.86	0.2	0.513	0.007	2668	13	100
1-Mar	286	120	0.43	0.27	0.181	0.0008	12.77	0.13	0.512	0.005	2662	8	100
14-1#	787	447	0.59	0.35	0.1742	0.0007	8.38	0.07	0.349	0.003	2599	7	135
26-1	96	22	0.24	0.31	0.1202	0.0016	5.93	0.11	0.358	0.005	1959	24	99
21-1	138	52	0.39	0.04	0.1121	0.0009	5.04	0.07	0.326	0.004	1834	15	101
Younger zircons													
1-Jun	137	145	1.09	0.08	0.108	0.0008	4.77	0.07	0.32	0.004	1765	14	98
19-1	152	75	0.51	0.12	0.1078	0.0008	4.8	0.06	0.323	0.004	1762	13	98
24-1	104	95	0.94	0.2	0.1066	0.0012	4.54	0.08	0.309	0.004	1742	21	100
1-May	468	452	1	0.3	0.1022	0.0007	4.15	0.04	0.295	0.002	1665	12	100
25-1	125	135	1.11	0.15	0.1006	0.0009	4.11	0.06	0.296	0.004	1635	17	98
1-Dec	60	86	1.47	0.12	0.0984	0.002	3.86	0.1	0.284	0.004	1595	38	99
22-1	157	122	0.8	0.09	0.0967	0.001	3.7	0.07	0.278	0.004	1562	19	99
13-1#	423	266	0.65	0.72	0.0823	0.002	2.2	0.07	0.194	0.004	1252	48	110
29-1	62	84	1.41	0.21	0.0795	0.0025	2.15	0.08	0.197	0.003	1185	63	102

Pb isotopic ratios are for radiogenic Pb after correction for common Pb (204-correction of Compston et al., 1984)

Conc. = concordance.

Reproducibility of U/Pb for BR266 zircon standard was +/-1.31% (2σ; n = 15).

discordance ≥10%: not considered in discussion of age data.